AD-A155 010 AN EXPERIMENT IN MIXING AND INTERFACIAL STRESS(U) ARMY 1/2
ENGINEER WATERWAYS EXPERIMENT STATION VICKSBURG MS
HYDRAULICS LAB G H KEULEGAN FEB 85 WES/MP/HL-85-1

UNCLASSIFIED F/G 20/4 NL

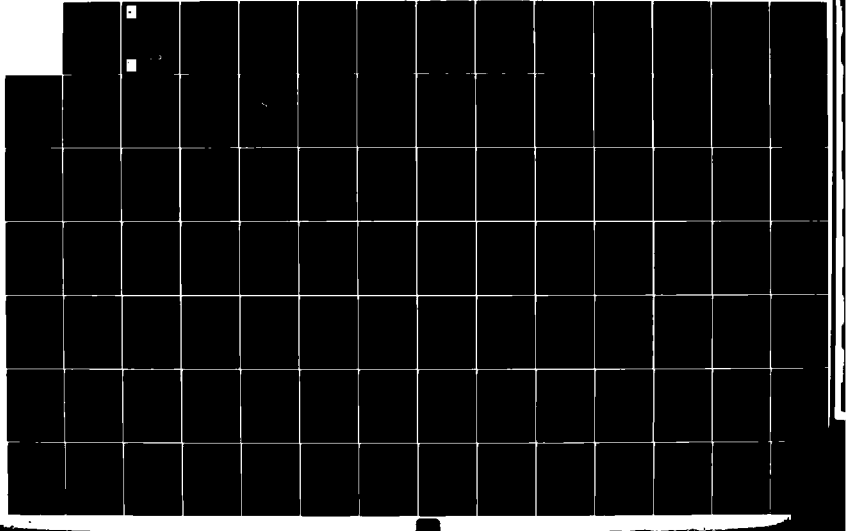

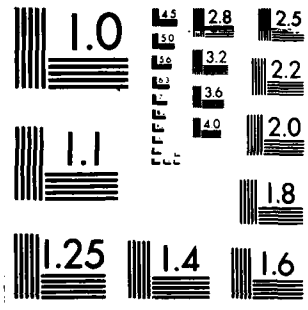

US Army Corps of Engineers

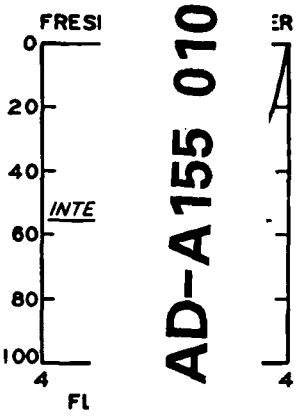

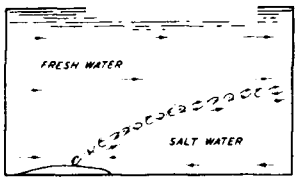

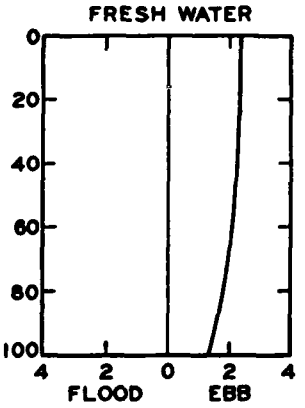

HYDRAULICS LABORATORY

(2)

MISCELLANEOUS PAPER HL-85-1

AN EXPERIMENT IN MIXING, AND INTERFACIAL STRESS

by

Garbis H. Keulegan

Hydraulics Laboratory

DEPARTMENT OF THE ARMY
Waterways Experiment Station, Corps of Engineers
PO Box 631
Vicksburg, Mississippi 39180-0631

February 1985
Final Report

Prepared for

DEPARTMENT OF THE ARMY
US Army Corps of Engineers
Washington, DC 20314-1000

Destroy this report when no longer needed. Do not return it to the originator.

The findings in this report are not to be construed as an official *Department of the Army position unless so designated* by other authorized documents.

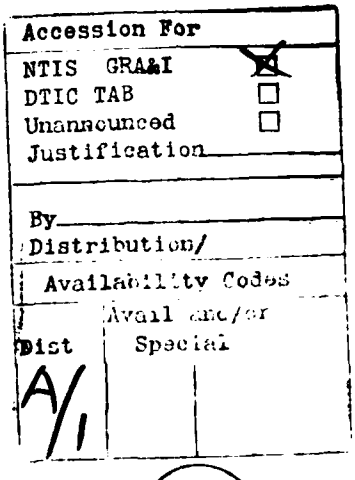

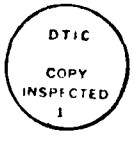

The contents of this report are not to be used for advertising, publication, or promotional purposes. Citation of trade names does not constitute an official endorsement or approval of the use of such commercial products.

Unclassified

SECURITY CLASSIFICATION OF THIS PAGE *(When Data Entered)*

REPORT DOCUMENTATION PAGE		READ INSTRUCTIONS BEFORE COMPLETING FORM
1. REPORT NUMBER Miscellaneous Paper HL-85-1	2. GOVT ACCESSION NO. AD-A155	3. RECIPIENT'S CATALOG NUMBER CCC
4. TITLE *(and Subtitle)* AN EXPERIMENT IN MIXING AND INTERFACIAL STRESS		5. TYPE OF REPORT & PERIOD COVERED Final report
		6. PERFORMING ORG. REPORT NUMBER
7. AUTHOR(s) Garbis H. Keulegan		8. CONTRACT OR GRANT NUMBER(s)
9. PERFORMING ORGANIZATION NAME AND ADDRESS US Army Engineer Waterways Experiment Station Hydraulics Laboratory PO Box 631, Vicksburg, Mississippi 39180-0631		10. PROGRAM ELEMENT, PROJECT, TASK AREA & WORK UNIT NUMBERS
11. CONTROLLING OFFICE NAME AND ADDRESS DEPARTMENT OF THE ARMY US Army Corps of Engineers Washington, DC 20314-1000		12. REPORT DATE February 1985 13. NUMBER OF PAGES 95
14. MONITORING AGENCY NAME & ADDRESS *(if different from Controlling Office)*		15. SECURITY CLASS. *(of this report)* Unclassified 15a. DECLASSIFICATION/DOWNGRADING SCHEDULE

16. DISTRIBUTION STATEMENT *(of this Report)*

Approved for public release; distribution unlimited.

17. DISTRIBUTION STATEMENT *(of the abstract entered in Block 20, if different from Report)*

18. SUPPLEMENTARY NOTES

Available from National Technical Information Service, 5285 Port Royal Road, Springfield, Virginia 22161.

19. KEY WORDS *(Continue on reverse side if necessary and identify by block number)*

Density currents (LC)
Fresh water--Experiments (LC)
Hydraulics (LC)
Saline waters (LC)
Saltwater encroachment (LC)
Water--Density--Measurement (LC)

20. ABSTRACT *(Continue on reverse side if necessary and identify by block number)*

The mixing characteristics between two layers, freshwater energy over a practically stagnant saline water, together with the average internal stress are examined in a laboratory channel. The vertical velocity distribution is examined at three stations equally separated. The distribution of velocities was examined only in the two sections. Entrainment is evaluated from density and velocity observations. The stress determinations are based on the flow equation of the saline water layer and the freshwater layer. In deriving the freshwater equation, care was taken to include terms arising from entrainment.

DD FORM 1 JAN 73 1473 EDITION OF 1 NOV 65 IS OBSOLETE

Unclassified

SECURITY CLASSIFICATION OF THIS PAGE *(When Data Entered)*

PREFACE

The study reported herein was completed in the Hydraulics Laboratory, US Army Engineer Waterways Experiment Station (WES), Vicksburg, Mississippi, as a portion of the Navigation Hydraulics Program being conducted for the Office, Chief of Engineers, US Army. The experimental work was completed at the National Bureau of Standards.

This report was prepared under the direction of Mr. H. B. Simmons, Chief of the Hydraulics Laboratory, by Dr. G. H. Keulegan, Special Assistant to the Chief of the Hydraulics Laboratory.

Commander and Director of WES during the preparation and publication of this report was COL Robert C. Lee, CE. Technical Director was Mr. F. R. Brown.

CONTENTS

AN EXPERIMENT IN MIXING AND INTERFACIAL STRESS

PART I: INTRODUCTION

1. The matter of mixing was one of the problems mentioned in the original letter from the Chief of Engineers to the Director of National Bureau of Standards, 19 December 1945, requesting studies on density current. Subsequently, a report on mixing in arrested saline wedges was issued (Keulegan 1955). The transport rate of saline waters into flowing fresh water above, U_{ml}, was shown to be proportional to $U-U_c$, where U is the average velocity of flowing fresh water and U_c the threshold critical velocity associated with the initiation of mixing. Suspecting that the simple result thus obtained may be lacking in general application, it was decided to examine the corresponding problem for the case where the upper fluid is flowing over a long pool of mainly stagnant saline water.

2. Although the experimental part of this study was completed in the spring of 1960, only recently the opportunity was presented to examine and to interpret the observational data. The main result is that the entrainment ratio U_m/U is practically independent of the densimetric Froude number. This is at variance with the recent investigations showing that this ratio instead of being a constant is a function of densimetric Froude number. This disparity possibly can be related to the flow end conditions. In this case, the present study might be of value and accordingly the procedures followed are given in great detail in order to facilitate the examination of the problem by other interested researchers.

PART II: EXPERIMENTAL SETUP

3. The lower downstream portion of a long flume 23 cm wide, connecting the forebay with the sea reservoir, was modified to form the experimental setup of 36.5-m length. Previously, the channel was employed to study the properties of arrested saline wedges. The entrance segment of the modification is shown in Figure 1; the exit segment, in Figure 2. The drawings are

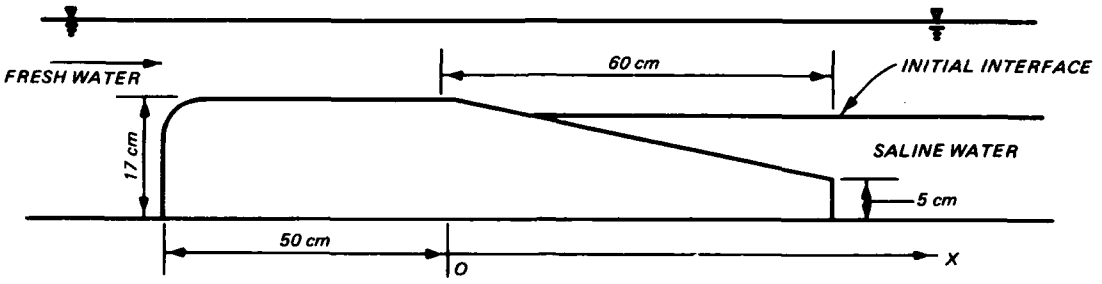

Figure 1. Entrance segment of experimental channel

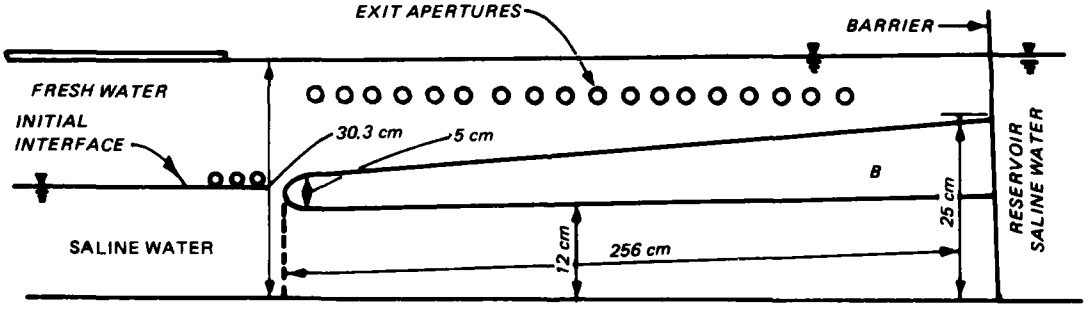

Figure 2. Exit segment of experimental channel

not to true scale. The sketch of the first is self-explanatory. In the second, a firm barrier plate separates the exit segment from the sea reservoir which in the present study served as the source of saline waters. Fresh water leaves the channel laterally through the exit orifices located on one of the channel sidewalls. There are eighteen 1/2-in.-diam (12.7 mm) holes that can be manipulated to maintain a water-surface elevation of 30.3 cm, measured from channel bottom, independent of freshwater discharge. In the manipulation, an open slit on one of the channel walls, 40 cm long and 2 cm deep with its lower brim 30 cm above the channel floor, is of considerable value. Thus

in all the runs of the study the total depth of the liquids, fresh and saline, at the segment is maintained at 30.3 cm. The discharging water is isolated from the saline waters below by means of the separating block B firmly attached to the barrier plate. During the tests, with increasing freshwater velocities the upstream end of the interface would be depressed and the downstream end at the exit segment would be elevated. In the tests chosen, the interfaces remained at the downstream end just above the rounded tip of the separating block.

4. The saline layer of the runs was prepared in the following manner. The channel was first filled with fresh water to a depth of 30 cm and next, the saline water was introduced laterally through small apertures at one of the channel walls. The apertures, eight in number, were distributed evenly along the channel and in line with the bottom of the channel. The connections with the saline reservoir were through small diameter hoses with capillary restrictions. The liquid surfaces in channel and saline reservoir being kept at the same level, the driving force for the flow in the hoses arises from the density difference of the two liquids. Thus saline water is allowed to slip slowly into the lower layer of fresh water in the channel. The flow is maintained until the interface reaches a level about 15 cm high. The interface finally obtained is far from being clear and distinct. The saline water is colored and as the channel walls formed from lucite are transparent, the condition of the interface can be examined by the eye with great ease. Introducing a weak freshwater discharge, affecting the efflux through small apparatus at one of the walls in the area of the tip of block B, the interface is made sufficiently clear to observe.

5. The fresh water for the tests emanates from a small constant-level tank with numerous efflux orifices at its base, placed over the forebay leading to the channel. The orifices consist of short brass tubes of various sizes and are calibrated in place by noting the time required to fill a channel segment of a given length to a desired depth. For the study, eight distinct discharges are employed, the least being 850 cm^3/sec and the largest, 7,692 cm^3/sec.

6. To prevent the excessive lowering of the interface during the vertical traverses, either of velocity or of density, due to the entrainment of saline waters, first the region under block B was connected with the saline reservoir through a short rubber hose of 1/2-in. (12.7 mm) internal diameter.

Next, as this arrangement was not found to be effective, the entrance area of the saline waters in the channel was connected with the saline reservoir through three rubber hoses of 1/2-in.-diam tubes. The driving force for the flows through the hoses is due to the differences of the vertically arranged densities of the liquids in the channel and the reservoir saline water. The flows through the hoses enter the channel laterally.

7. A rectangular trough, 5 cm wide, 3 cm high, and 33 m in length, is attached horizontally to one of the walls of the channel. This is used to measure fall of free surface. It is connected with the channel at midstation, and the water in the trough is of the same elevation as the channel surface water at midstation at all times. The surface fall is determined by means of optical manometers to be discussed later.

PART III: PROCEDURES AND MEASUREMENTS

Slope of Interface

8. Interface heights, h_s, are observed visually against 10 paper scales attached to the outside surface of one of the channel walls at equal intervals. Due to parallax, the readings could be in error as much as 2 mm. This is ignored. Initially the interface is horizontal, but soon after fresh water of a chosen Q is introduced, the interface at the entrance segment commences to fall. This is due to the fact that in the main the saline water is stagnant, and the frictional force of the moving water is subsequently balanced. In the runs, the interface height of the exit segment tended to each a constant value irrespective of the freshwater velocities. For saline water relative densities $\Delta\rho_s$ = 0.02, 0.04, and 0.06, the heights were 17.1, 18.9, and 17.2 cm, 80 cm upstream of the separating block. Definitely, the saline height of the area is controlled by the geometry of the exit segment. At the entrance segment, saline water heights decrease with increasing freshwater discharges. Neither of the two ends is a critical section.

9. For small freshwater discharges, saline water height increases uniformly. For large discharges, the increase of height is not uniform and the rate of increase is augmented with distance. Data of Figure 3 are an example. Whether this behavior is related to the actual flow mechanism or is brought about for difficulty of observation of a diffused interface picture due to severe turbulence is not clear. In this case, the initial rate of increase is taken to represent the interface slope. Data on the interface slope in the tests where both the fall of surface waters and the interface heights are observed are collected in Table 1. The slope of interface is related to densimetric Froude number as shown in Figure 4. Data are based on evaluations entered in Table 2. Some scatter of points is present with the data for $\Delta\rho_s$ = 0.04 being displaced higher than the rest. Yet disparities are not systematic and the straight line drawn yields the relation:

$$\frac{dh_s}{dx} = C \frac{U^2}{\frac{\Delta\rho_s}{\rho} g h_w} \quad , \quad C = 1.11 \times 10^{-2} \tag{1}$$

Here, U is the water mean velocity computed from

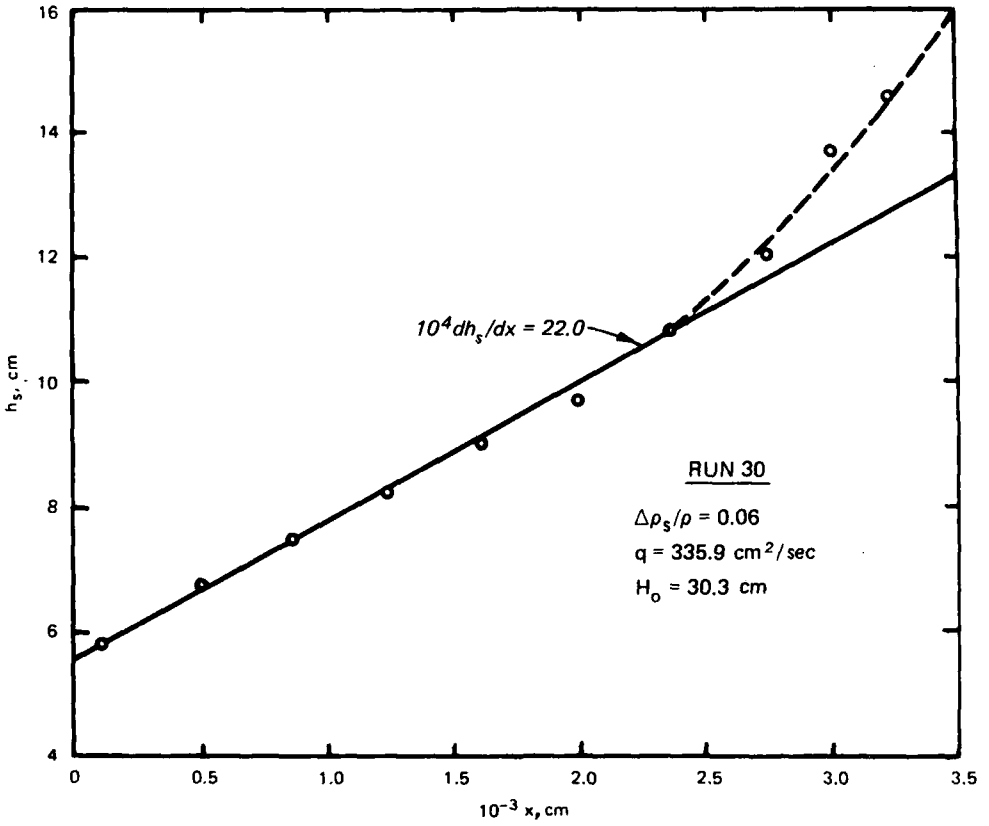

Figure 3. An example of variation of interface height with distance

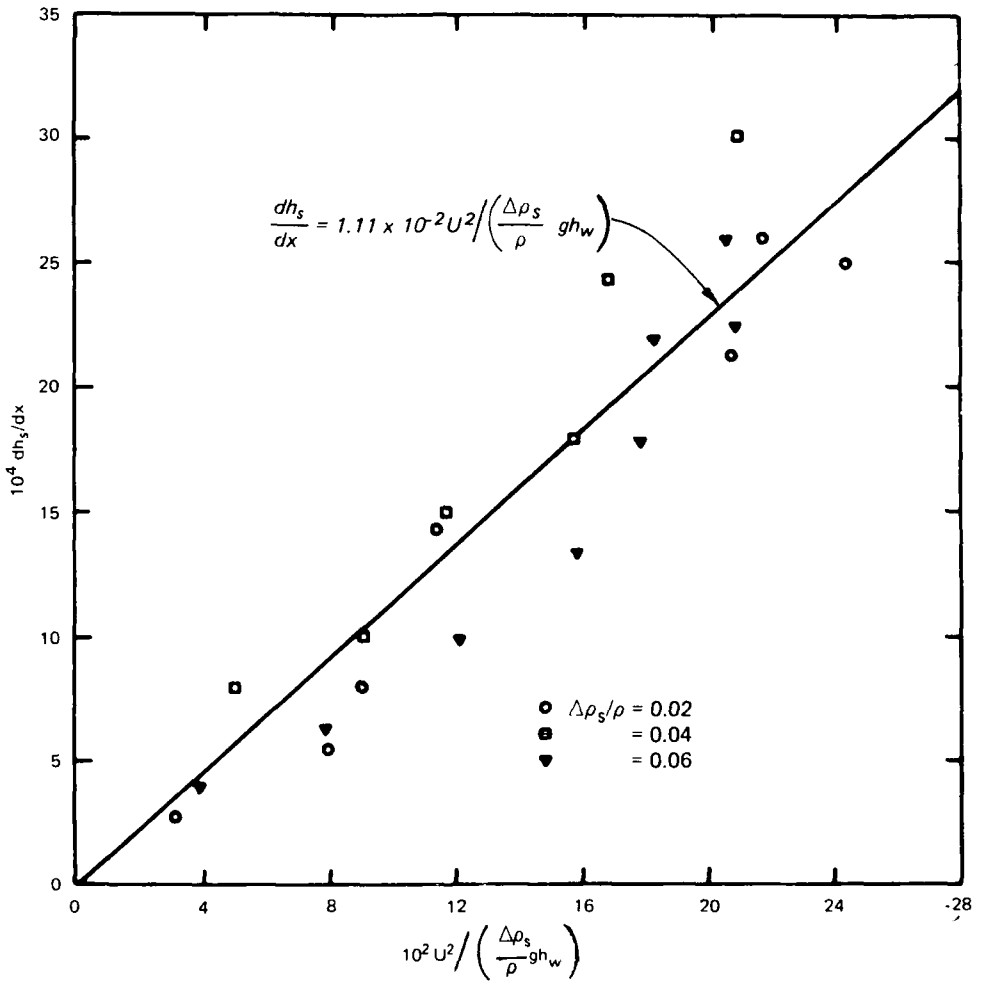

Figure 4. Variation of interfacial slope with densimetric Froude number

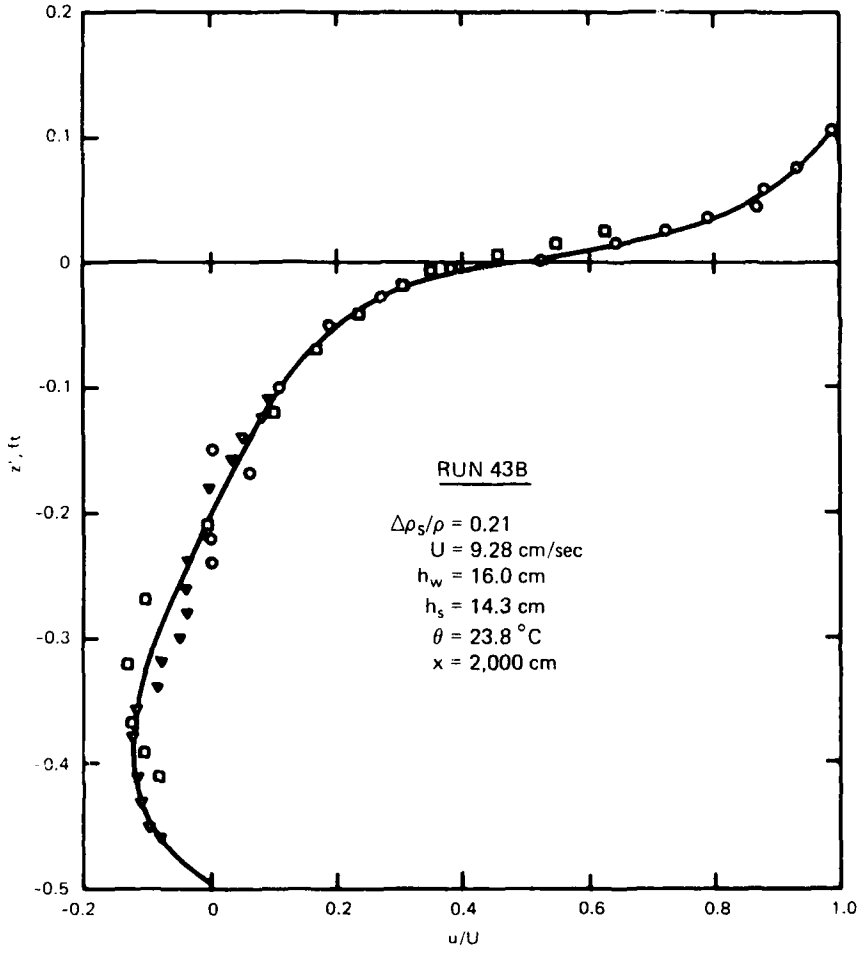

Figure 13. An example of velocity distribution in saline water layer

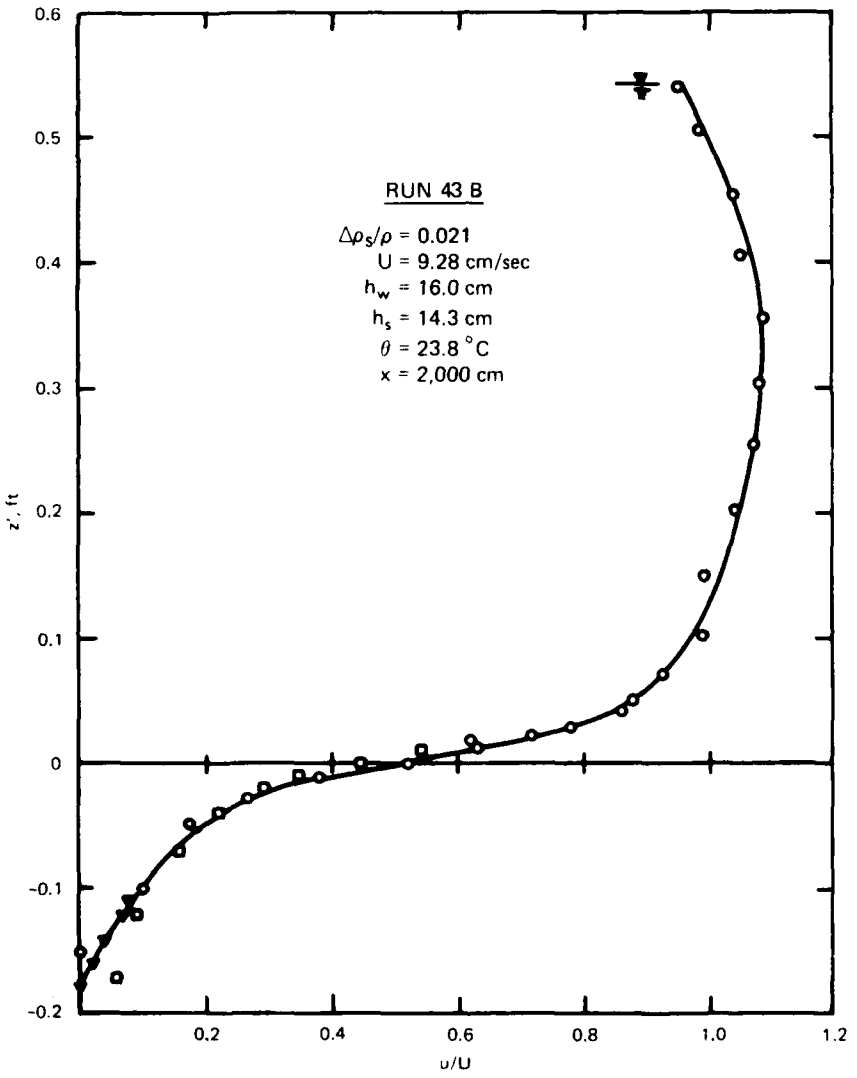

Figure 12. An example of velocity distribution in freshwater layer

$$\kappa = \frac{E^{1/2} t^{3/2}}{\sqrt{2}\rho^{1/2} \ell^2} \tag{24}$$

In the actual use of a ribbon, however, κ, instead of being based on this last relation, was determined by using the summation of $\delta^{1/2}$ readings in a traverse from the freshwater surface down to the interface in accordance with

$$U = \frac{\kappa}{h_w} \int_0^{h_w} \delta^{1/2} \, dz' \tag{25}$$

Here z' is the distance measured from the interface, h_w the depth of freshwater layer, and U the current mean velocity. Small velocities of the saline water layer were measured mostly using lucite ribbons while phosphor bronze ribbons were reserved for the freshwater velocities.

Fresh and Saline Water Velocities

18. Examples of fresh and saline water velocity measurements are shown in Figures 12 and 13, respectively. Drawing smooth curves through the data points for a selected abscissa u may be read to form the ratio u/U, U being the current mean velocity obtained as $U = q/h_w$. The relative velocities of the freshwater area, from the runs with $\Delta\rho_s/\rho = 0.04$ and observed at $x = 2{,}000$ cm, are shown in Table 3. It is evident that the pattern of velocities, u/U as a function of z'/h_w, is hardly affected by the current velocity in the range from 5.5 cm/sec to 14.10 cm/sec. The averages are shown in the last column. Similar behavior is noted in the measurements of the runs with $\Delta\rho_s/\rho = 0.02$ and $\Delta\rho_s/\rho = 0.04$. The averages from all these tests are shown in Table 4. There are only small differences in the entries for a given z'/h_w and thus it would be appropriate to take the averages shown in the last column as the characteristic pattern of freshwater velocities independent of the mean current velocity and the saline water density. The graph of the average is shown in Figure 14 and the latter will be utilized in the entrainment analysis.

19. The values of u/U in the saline water area from the corresponding

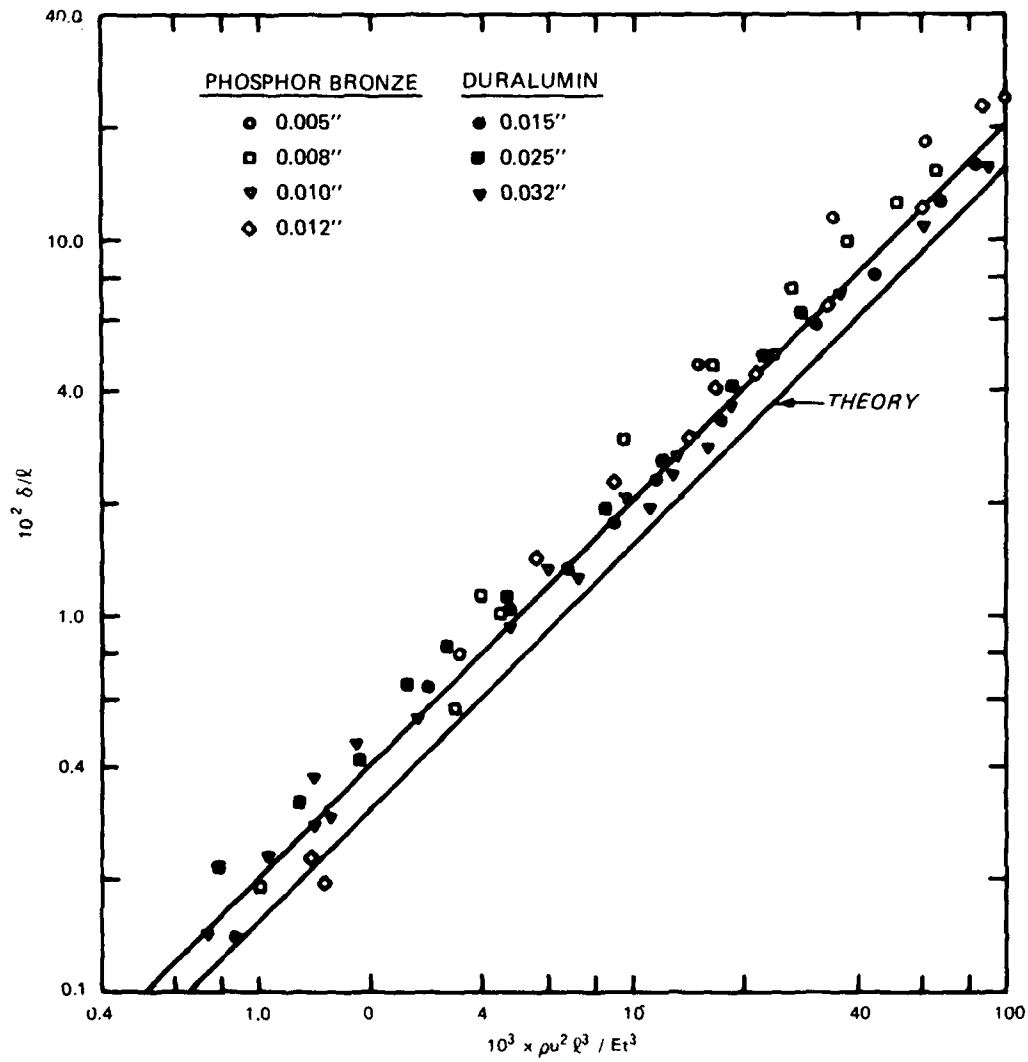

Figure 11. Dependence of deflection of immersed ribbon on current velocity

$$\eta = \Pi\left(\frac{\zeta^2}{2} - \frac{\zeta^3}{3} + \frac{\zeta^4}{12}\right) - \frac{1}{6}\int_0^{\zeta}\left(\frac{d\eta}{d\zeta}\right)^3 d\zeta - \Pi\int_0^{\zeta}\int_0^{\zeta}(1-\zeta)\int_{\zeta}^{1}\left(\frac{d\eta}{d\zeta}\right)^2 d\zeta\, d\zeta\, d\zeta \quad (19)$$

since η and $\frac{d\eta}{d\zeta}$ vanish at $\zeta = 0$, due to the manner ribbon is attached to gage vertical stem. Obviously, a first approximate solution is:

$$\eta = \Pi\left(\frac{\zeta^2}{2} - \frac{\zeta^3}{3} + \frac{\zeta^4}{12}\right) \quad (20)$$

and the analysis may be continued evaluating the second and the third terms using the approximate value of η. The rest is just so much algebra; the steps will be omitted here. Finally, the end reflection on this basis is

$$\frac{\delta}{\ell} = 0.25\Pi - 0.025\Pi^3 \quad (21)$$

17. During the spring of 1956, H. L. Carpenter, a previous colleague of mine, studied experimentally the behavior of ribbons subjected to currents using the same channel as of the present investigation. The ribbons selected were of phosphor bronze and Duralumin material, 21.3 cm in length, of 1/4-in. width and of various thicknesses. The ribbons were placed in currents with water depths from 3 to 5 cm and at such distances from the channel bottom that the point velocities would be the same as the mean velocity. Such distances were determined on the basis of Blasius velocity law. The scale to read deflections was pasted on the outside wall of the channel. Zero of scales was read with water still in the channel. Results from this study are shown in Figure 11 together with the theoretical determination evaluated from Equation 21. The alignment of the experimental points is linear leading to a straight line slightly above the theoretical line. The former may be described as

$$\frac{\delta}{\ell} = 2.0\,\frac{\rho u^2 \ell^3}{Et^3} \quad (22)$$

This suggests that the relation between δ and u may be expressed as

$$u = \kappa\delta^{1/2} \quad (23)$$

The flexural deformation of ribbon is in accordance with

$$M = \frac{bEt^3}{12R} \tag{13}$$

where E is the modulus of elasticity of ribbon material, t the ribbon thickness, and R the radius of curvature at s,

$$\frac{1}{R} = \frac{d^2y/ds^2}{\sqrt{1 - \left(\frac{dy}{dx}\right)^2}} \tag{14}$$

Since it was assumed that dy/ds is small, the latter becomes

$$\frac{1}{R} = \frac{d^2y}{ds^2} + \frac{1}{6}\frac{d}{ds}\left(\frac{dy}{ds}\right)^3 \tag{15}$$

The combination of Equations 12, 13, and 15 leads to

$$\frac{d^2y}{ds^2} = \frac{3\rho C_D u^2}{Et^3}\left[(\ell - s)^2 - (\ell - s)\int_s^\ell \left(\frac{dy}{ds}\right)^2 ds\right] - \frac{1}{6}\frac{d}{ds}\left(\frac{dy}{ds}\right)^3 \tag{16}$$

Introducing

$$\eta = \frac{y}{\ell}$$

$$\zeta = \frac{s}{\ell} \tag{17}$$

$$\Pi = \frac{3\rho C_D u^2 \ell^3}{Et^3}$$

Equation 16 transforms to

$$\frac{d^2\eta}{d\zeta^2} = \Pi\left[(1 - \zeta)^2 - (1 - \zeta)\int_\zeta^1 \left(\frac{d\eta}{d\zeta}\right) d\zeta\right] - \frac{1}{6}\frac{d}{d\zeta}\left(\frac{d\eta}{d\zeta}\right)^3 \tag{18}$$

Integrating the terms of the equation with respect to ζ twice, between limits $\zeta = 0$ and $\zeta = \zeta$

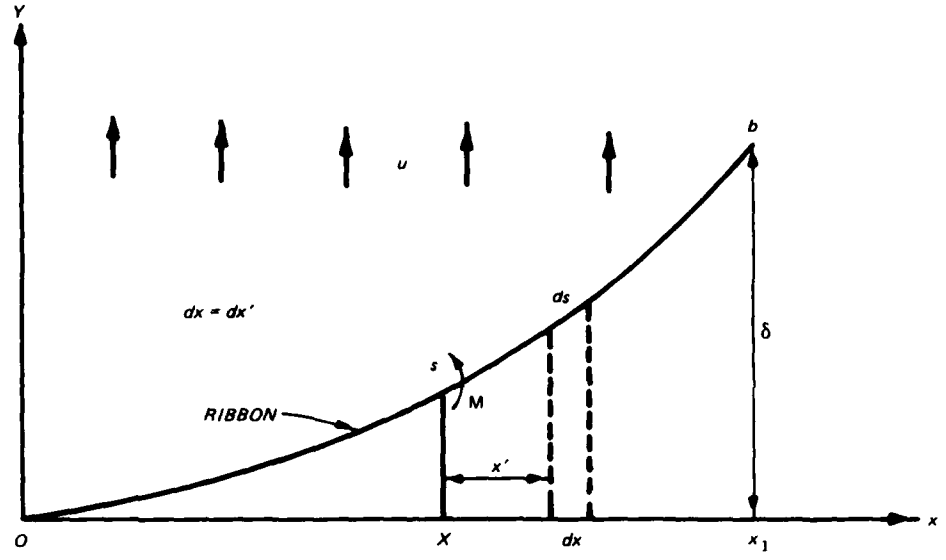

Figure 10. Deflection of ribbon in flowing liquid

The total moment on the cross section at s due to the moment of the forces acting as the part of ribbon between s and ℓ, ℓ the length of ribbon, would be

$$M = \rho b C_D \frac{u^2}{4} (x_1 - x)^2 \tag{10}$$

In terms of s, since

$$x = \int_0^s \left(\frac{dx}{ds}\right) ds$$

the moment is

$$M = \frac{\rho b C_D u^2}{4} \left\{ \int_s^\ell \left[1 - \left(\frac{dy}{ds}\right)^2 \right]^{1/2} ds \right\}^2 \tag{11}$$

Restricting attention to the case where dy/ds is small with respect to unity

$$M = \frac{\rho b C_D u^2}{4} \left[(\ell - s)^2 - (\ell - s) \int_s^\ell \left(\frac{dy}{ds}\right)^2 ds \right] \tag{12}$$

curves coalesce. Since $H_o = h_s + h_w$, very nearly, the curve of Figure 9 suggests the relation

$$\frac{d\delta}{dx} = 0.012 \frac{U^2}{gh_w} \left(1 + \frac{h_s}{h_w}\right)^{-1} \tag{7}$$

The Method of Velocity Measurements

15. Fresh and saline water velocities are measured by noting the end deflection of a thin metallic ribbon held normal to the flow direction. The length of the ribbon is just slightly less than the width of channel. Attached to the stem of a measuring gage, it may be raised or lowered to any position. The scale for the deflections, attached to a second gage, may be also raised or lowered to any position. The zero of the ribbon is noted after raising the ribbon and the scale just slightly above the water surface. It is assumed that in lowering the ribbon and the scale into the fresh water, on the saline water the scale zero reading is not changed. This is not certain. Possibly low velocity readings are open to error. At the time it was realized that this difficulty may be eliminated by mounting a strain gage at the fixed end of the ribbon. However, this meant a new effort to develop the new device. Lacking the time for it the idea was relegated. In what follows, the elastic theory of the ribbon will be developed (Figure 10).

16. The force on an element of ribbon of length ds having the projection dx and dx' normal to the flow is

$$\Delta F = \rho b C_D \frac{u^2}{2} dx \tag{8}$$

where ρ is the density of liquid, b the width of ribbon, C_D the drag coefficient, and u the current velocity. The coefficient C_D may be taken as 2. The corresponding bending moment on a section at a point of distance s measured along the length of the ribbon would be

$$\Delta M = \rho b C_D \frac{u^2}{2} x' dx' \tag{9}$$

where x' is the distance from x, the abscissa value corresponding to s.

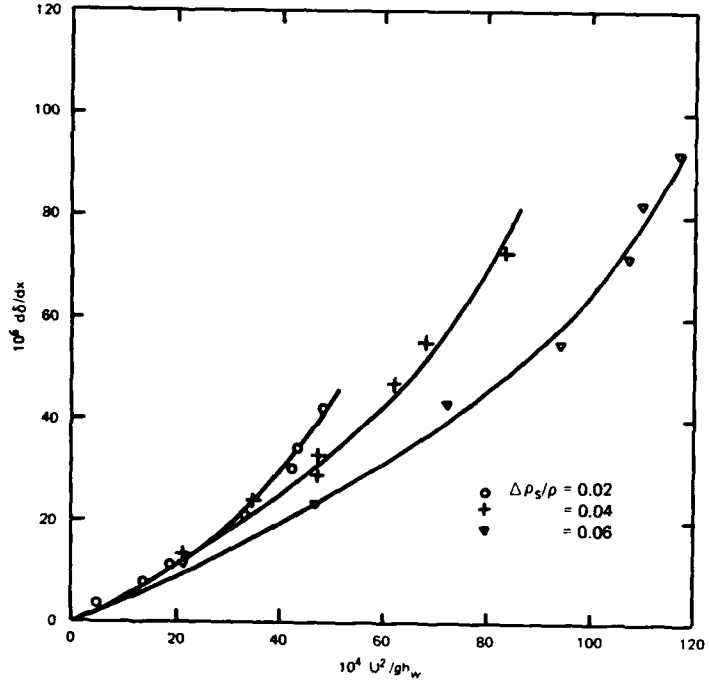

Figure 8. Dependence of the rate of fall of free surface on Froude number based on freshwater depth

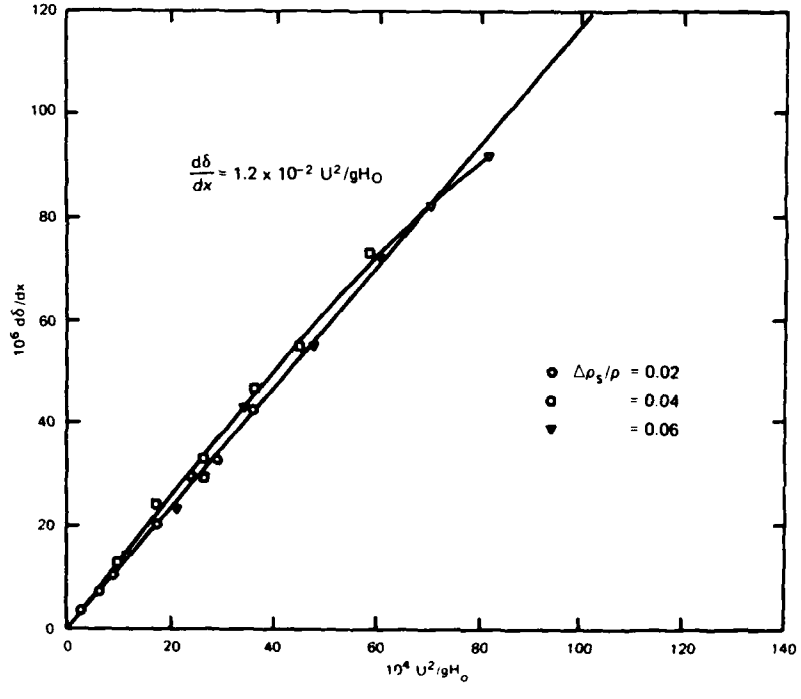

Figure 9. Dependence of the rate of fall of free surface on Froude number based on liquid total depth

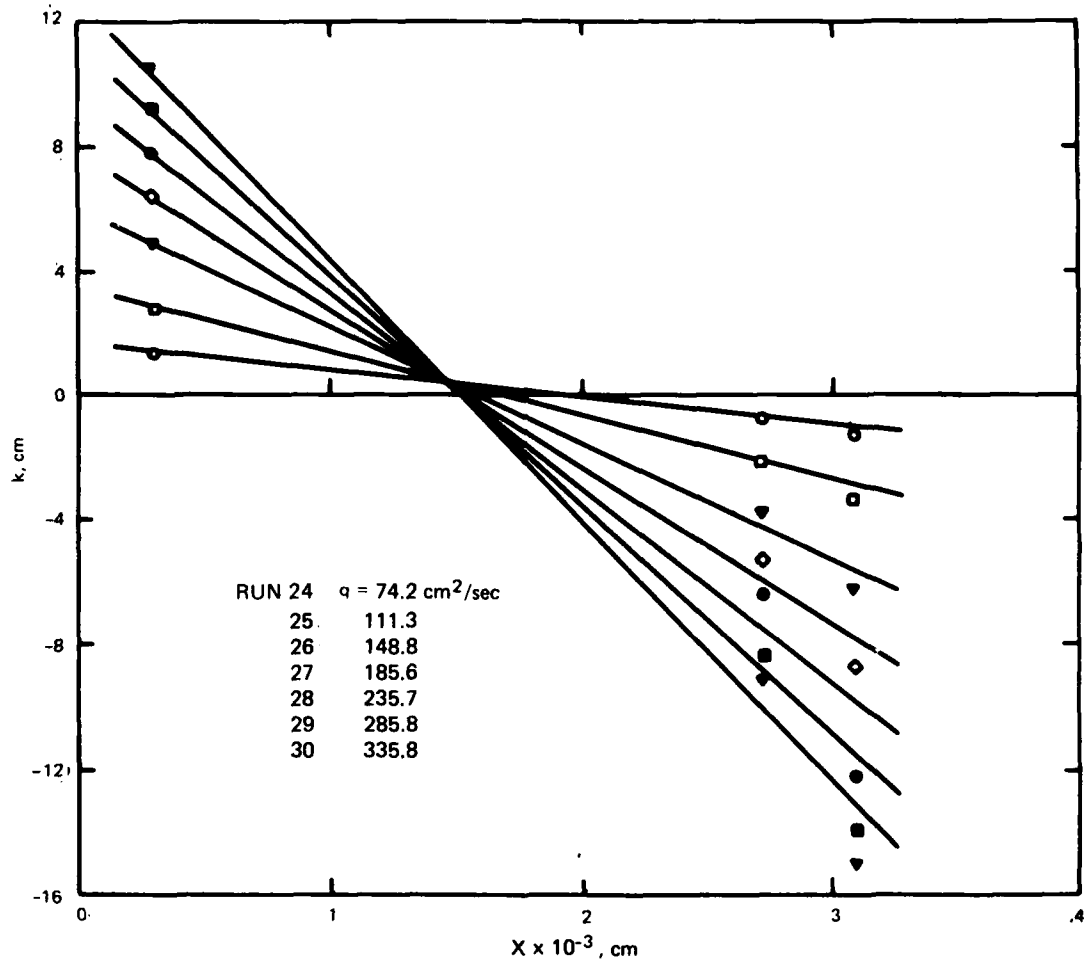

Figure 7. Fall of surface waters magnified, $k = 88\delta$

x_2 = 2,723 cm, and x_3 = 3,080 cm. A more efficient use of the manometers requires that each manometer is provided with an individual telescope and scale firmly placed. In this case, a zero of scale is readily obtained. Unfortunately, only one telescope was available at the laboratory which necessitated that the telescope and the accompanying scale be mounted on a table and the whole assembly be moved from one manometer location to the other, keeping the distance between scale and channel constant. In this procedure, an accurate zero cannot be had and the difficulty is overcome as follows. With the telescope facing a manometer, the frontal cell is connected with the trough along the channel and the hinder cell with the channel. Scale reading R_1 is noted. Next the connections are reversed, that is, the frontal cell is connected with the channel and the hinder cell with the trough and scale reading R_2 is noted. In this way the indication of fall of water surface in the channel, R , with respect to the water surface in the trough is doubled, that is $R_2 - R_1 = \Delta R = k$. The connection of the trough with channel waters is believed to be at $x = 1{,}610$ cm and thus ΔR would be positive for the first manometer and negative for the remaining two.

13. The readings R_1 and R_2 for a manometer were taken repeatedly for a period of 20 min. Averaged values are taken as representative. The resulting indications k obtained during the runs with $\Delta\rho_s/\rho = 0.06$ are shown in Figure 7 as an example. It appears as if the rate of surface fall δ is far from being uniform and increases in the downstream direction, especially when freshwater discharge is large; but an admissible value for the surface fall is obtained as follows. Denoting the magnified values of the surface fall with respect to waters in the trough by k_1, k_2, and k_3 corresponding to the manometer positions x_1, x_2, and x_3 , respectively, the effective surface fall is:

$$88\,\frac{d\delta}{dx} = \frac{1}{2}\left(\frac{k_1 - k_2}{x_2 - x_1} + \frac{k_1 - k_3}{x_3 - x_1}\right) \tag{6}$$

Determinations made in this manner are shown in the last column of Table 1.

14. Dependence of the rate of all $d\delta/dx$ on the Froude number based on the mean velocity of flow and the depth of freshwater layer is indicated in Figure 8. Data are taken from Table 2. The curves corresponding to three saline waters show disparities at greater freshwater discharges. On the other hand, when the Froude number is based on total depth H_o the individual

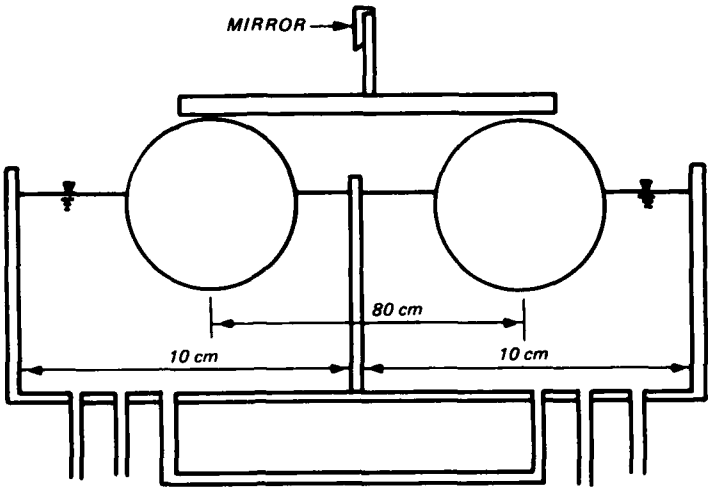

Figure 6. Optical manometer; cylinder length 10 cm, cell length 16 cm

manometer mirror by S and the scale reading by R, by geometry

$$2\frac{\delta_c}{s} = \frac{R}{S} \tag{5}$$

Thus the magnification of displacment δ_c is $M = 2(S/s)$.

11. Imperfect meniscus formation along the cylinder surfaces must be avoided for the satisfactory operation of the manometers. Although this will be somewhat less significant when the floating cylinders are made from hydrophobic material, for added precaution, however, small amounts of aerosol are added to the water of the manometer cells. The value of the magnification M is obtained by calibration instead of relating to geometry through Equation 5. First, water levels of the two cells are equalized by opening the connection between them and closing the connection with trough and channel. Scale reading R_1 is noted. Next, the connection between the two cells is closed and water of volume 5 cm^3 is introduced into the frontal cell. The new scale reading R_2 is noted. The basin area of each cell is 160 cm^2 and the resulting difference in heights of the water levels in the cells is 5/160. Thus the manometer magnification is $160(R_2 - R_1)/5$. For the three manometers, calibration yielded the values 44.9, 43.4, and 44.0. The value $M = 44.0$ is adopted as applying to all the manometers.

12. The manometers were located at the stations $x_1 = 300$ cm,

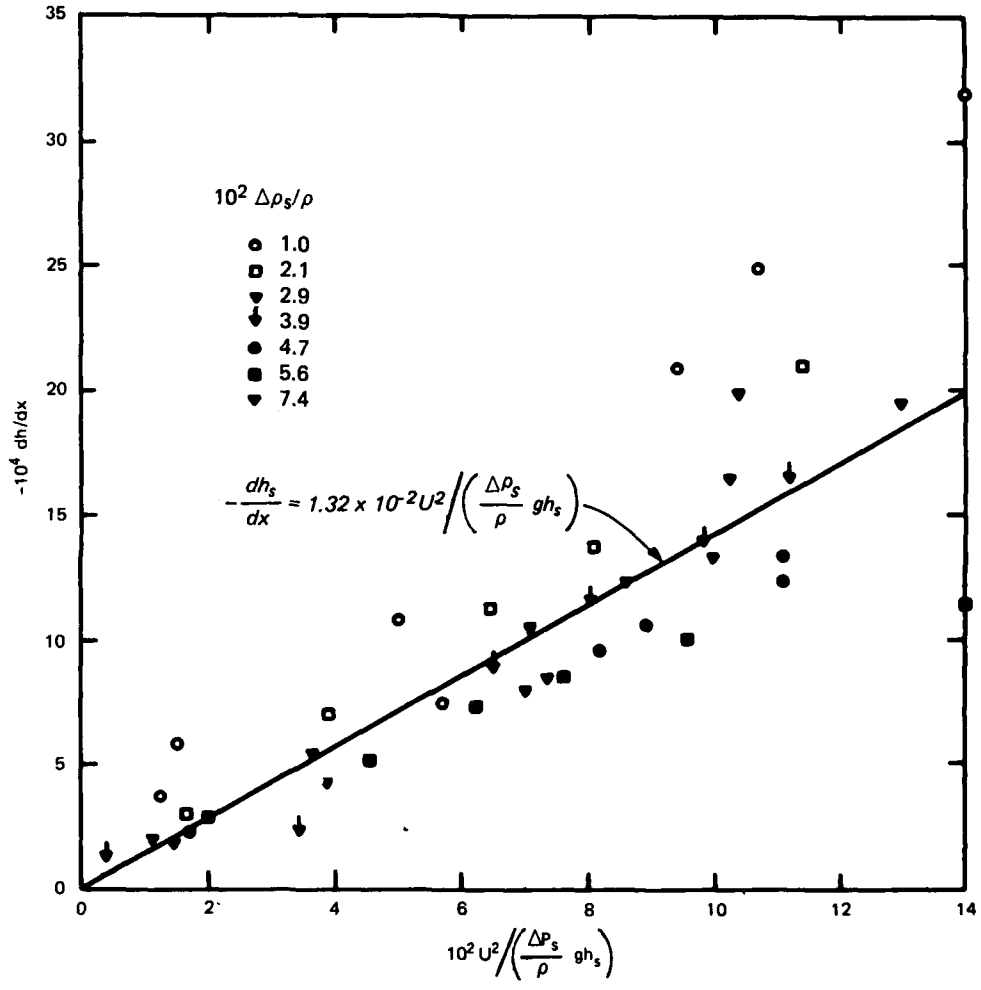

Figure 5. Variation of interfacial slope with densimetric Froude number (after Loftquist 1960)

$$U = \frac{q}{h_w} \tag{2}$$

where h_w is the freshwater depth at $x = 1{,}600$ cm, q the freshwater discharge per unit width of flume, ρ the density of water, and $\rho + \Delta\rho_s$ the density of salt water. Ignoring the fall of surface waters,

$$h_w = H_1 - h_s \tag{3}$$

As mentioned before, H_1, the total depth of the two layers at the exit segment, is of constant value 30.3 cm for all the tests of the study. Loftquist (1960) studied the mechanism of underflow in this same channel where the present study was carried out. In this case, the interface would be falling and one may deduce from these data (Figure 5) the relation

$$-\frac{dh_s}{dx} = C\,\frac{U^2}{\frac{\Delta\rho_s}{\rho} g h_s} \qquad C = 1.35 \times 10^{-2} \tag{4}$$

where U is the mean flow velocity of saline water below h_s, the depth of saline underlayer. Agreement of these two results is close.

Fall of Surface Waters

10. The fall of surface waters is measured with three optical manometers, each consisting of two cells that may be connected with each other, with the small trough running along the length of channel, or with the main channel itself. Details of construction are shown in Figure 6. Two lucite cylinders, the ends closed, are attached to a rectangular platform with a thin stem projecting upward on which a galvanometer mirror is attached. Distribution of the masses is such that when the waters of the cells are in the same horizontal plane, the center lines of the two cylinders would be also in the same level. The differential of the levels of the waters in the cells would lead to a rotation of mirror surface. This could be translated into a scale reading using a telescope with a vertical scale next to it. Let s be the distance between the cylinders and δ_c the relative displacement of the waters in the cell. The resulting rotation of the mirror surface is δ_c/s. Denoting the distance of the telescope scale from the

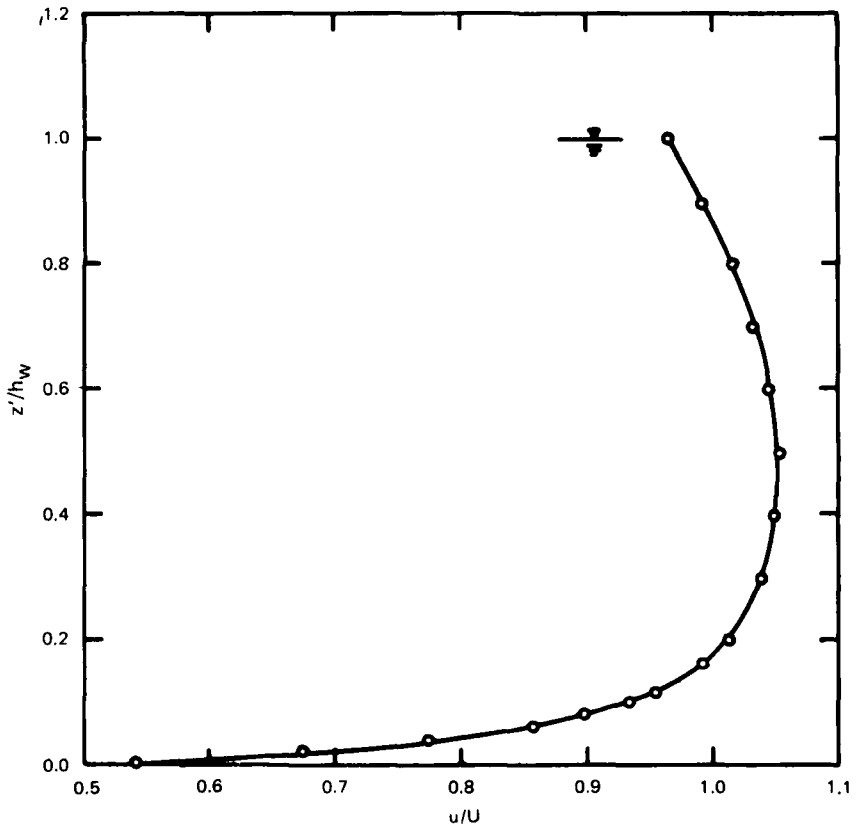

Figure 14. Characteristic curve of velocities in freshwater layer

runs are shown in Table 5. From column to column there are some differences in the u/U values for a given elevation z'/h_s. These are probably due to observation difficulties, mainly from the uncertainties of the scale zero to read ribbon deflections. With this in mind it is appropriate to consider averages as shown in the last column. This average together with those from runs relating to $\Delta\rho_s/\rho = 0.02$ and $\Delta\rho_s/\rho = 0.04$ are shown in Table 6. It would be appropriate to take the average values shown in the last column (plotted in Figure 15) as being the characteristic velocity pattern for the saline water layer independent of current velocity and saline water density.

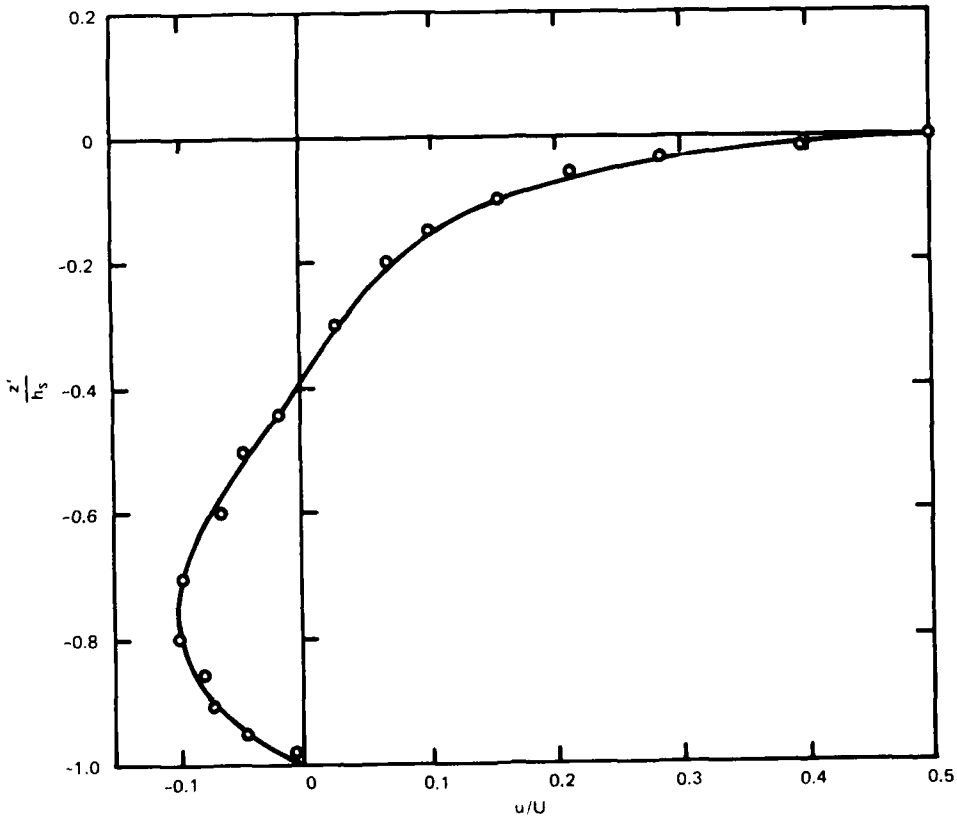

Figure 15. Characteristic curve of velocities in saline water layer

20. The above discussions relate to the velocities observed at station x = 2,000 cm. In addition to these, in separate tests, the velocities at station x = 3,000 were also investigated. The main results from the fresh water are shown in Figure 16. The curve drawn is reproduced from Figure 14. The close agreement of the data points with the curve suggests that there is similarity in the velocity pattern from section to section. The case for the saline water area is shown in Figure 17 and the curve likewise is reproduced from Figure 15. Complete similarity, here, does not exist. Data indicate that there is at the farther downstream cross section an effective flow to the right. This would be indicative of a pressure buildup in the area of channel exit. Owing to the smallness of ribbon deflection and of possible zero errors, we are not altogether certain of this.

Interfacial and Free Surface Velocities

21. The nature of the freshwater velocities is an important item in the evaluation of entrainment carried out subsequently. It was concluded in the above that in this particular area the velocity patterns are similar to each other at different cross sections. Interfacial and free surface velocities should be parts of this picture.

22. The surface velocities were measured by placing small paraffin particles on the central part of water surface and noting the travel time over selected distances. The values noted in the runs with saline waters of relative density difference $\Delta\rho_s/\rho = 0.06$ are shown in Table 7. In this, U_s/U denotes the ratio of surface velocity to the average current velocity U at sections of relative distance x/L, the ratio of section distance to the total length of saline pool under fresh water. Averaging the results obtained with varying current velocites U and adding the corresponding ones from the runs with $\Delta\rho_s/\rho = 0.02$ and 0.04 are shown in Figure 18a. The line drawn yields the value $U_s/U = 1.08$; but the corresponding value from Figure 14 is 0.98. The difference in these two values may be attributed to the fact that the paraffin particles measure the maximum of U_s , whereas the ribbon measures the mean root square of U_s across the entire width of channel.

23. For the observation of the interface velocities a globule of butyl phthalate dissolved in xylene, with a density equal to half that of saline

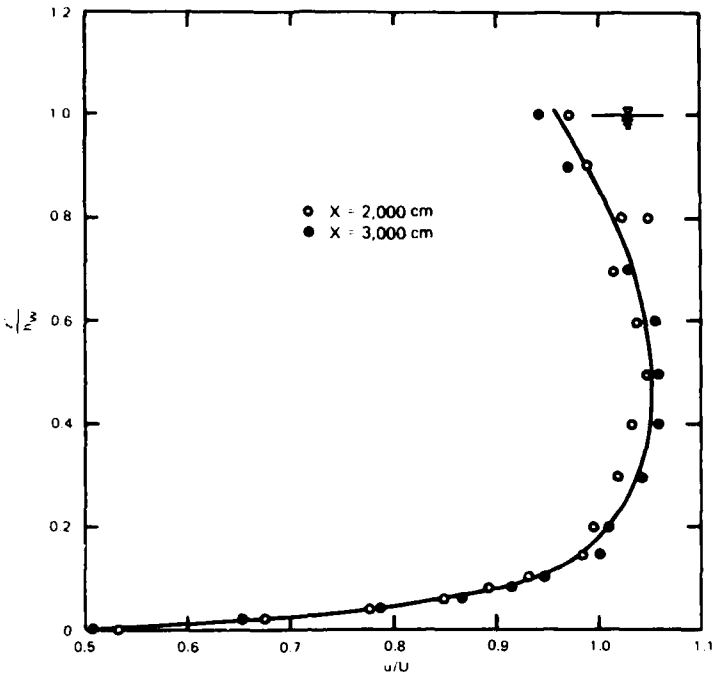

Figure 16. Characteristic curve of velocities in freshwater layer

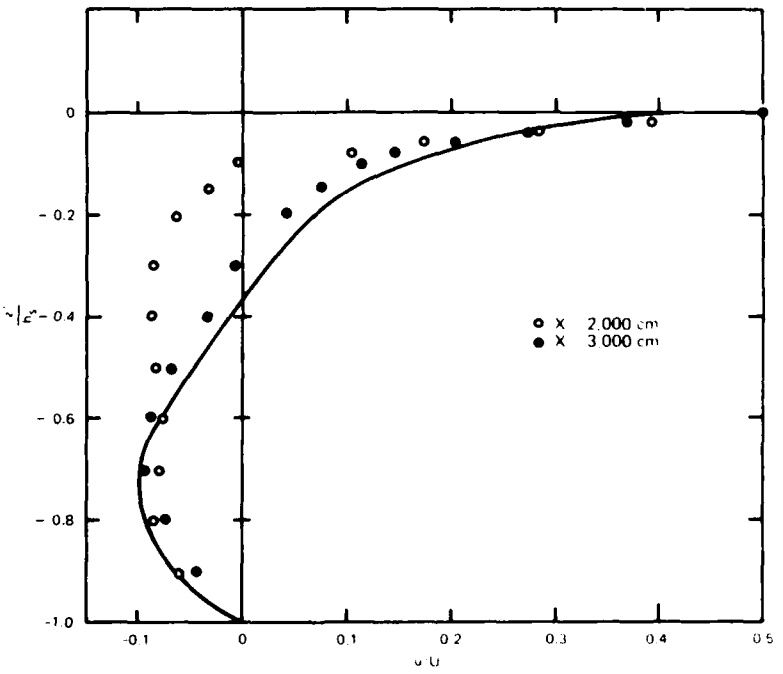

Figure 17. Characteristic curve of velocities in saline water layer

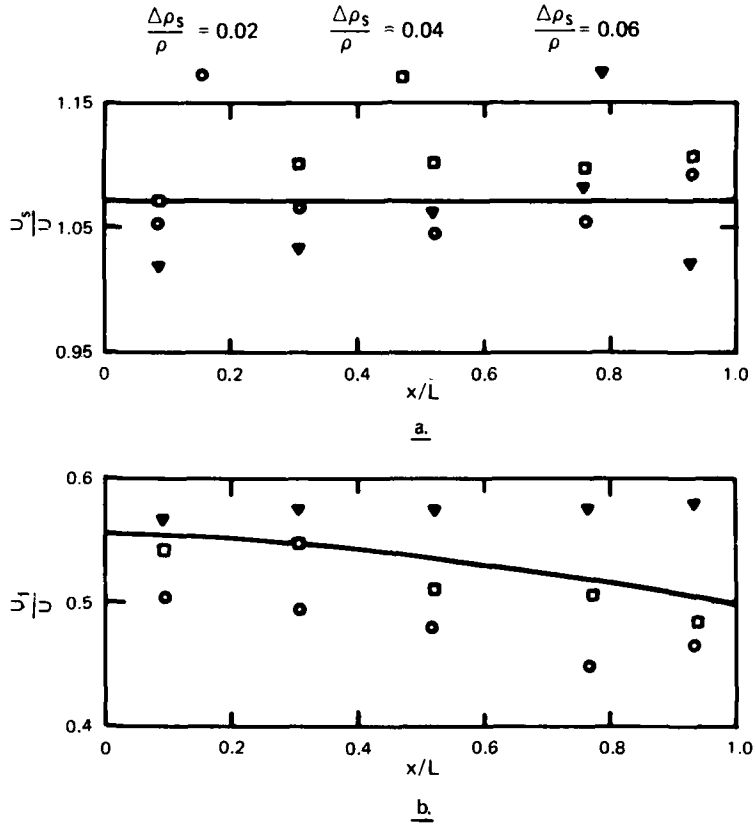

Figure 18. Interfacial and free surface velocities

water of a particular run, is injected by means of an eye dropper into the water a few centimeters below the surface. The size of the globule may be controlled by the diameter of the dropper opening. The globule diameters fell within the range of 3 to 6 mm. After the descent of the drop is completed, reaching the interface, the subsequent motion of the drop from one locality to another is timed. Let U_i be this interface velocity observed at the point x and U be the mean velocity of fresh water in the cross section through x. Forming the ratio U_i/U, observed values from tests with $\Delta\rho_s/\rho = 0.06$ and with varying freshwater velocities are shown in Table 8, as an example. For a given x/L, from one column to the other, values reveal only small differences. These differences may be ignored and the average taken to represent the group. These U_i/U averages and the similar ones from runs relating to saline water relative density differences $\Delta\rho_s/\rho = 0.02$ and 0.04 are shown in Figure 18. There are small differences in the U_i/U values for a given x/L. As these are not related to $\Delta\rho_s/\rho$, we take the curve drawn to be of general application. Thus independent of interface locality, saline water density, and freshwater current velocity, U_i/U equals 0.54.

Density Probe

24. Densities are determined directly by a traversing probe, the exploring end consisting of two parallel copper or platinum wires, 2 cm in length, 0.8 mm in diameter, and the spacing between them 0.5 cm. A small transformer provides the electromatic force, 6 volts, and the alternating current through the electrodes is measured by an a-c ammeter with shunts for various sensitivities.

25. The salinity of an electrolyte is related to the resistance between two parallel wires immersed in the solution. If the spacing between the wires is small, the resistance is given by

$$R = \frac{\tau}{\pi L} \log_e \left[\frac{2S}{d} \left(1 - \frac{d^2}{4S^2} \right) \right] \qquad (26)$$

where R is the effective resistance in ohms, τ the specific resistance of the electrolyte in ohms cm, L the length of the individual wires, d the diameter of the wires, and s the spacing of them, all measured in

centimeters. The above formula which should apply only to wires of great length is used to guide the design of the probe. The probe is calibrated with standard solutions of known densities. The above equation is due to Keulegan (1949).

26. The probe body consists of a flat rectangular lucite bar 1/4 in. thick and 13 in. long. Attached to a gage, the narrow edge faces the current. The electrode wires, located horizontally below the bar, are normal to the bar. The vertical movement of the gage allows a complete traverse from the channel bottom to the water surface. In the area of the interface, the densities are determined at intervals of 0.01 ft. In this, the determination of the exact locale of the interface line, $\Delta\rho/\Delta\rho_s = 0.5$, may be open to an error of 0.005 ft.

Effective Interface Layer Thickness

27. Following Loftquist (1960), the effective interface layer thickness may be defined by the relation

$$-\left(\frac{d\Delta\rho}{dz}\right)_{max} = \frac{\Delta\rho_s}{l_\rho} \tag{27}$$

after denoting the density of liquid at z by $\rho + \Delta\rho$. The graphic determination of l_ρ is illustrated in Figure 19. The evaluation made for the three saline water relative densities, $\Delta\rho_s/\rho = 0.02$, 0.04, and 0.06, are shown in Table 9. Values change only slightly with current velocities. The averages corresponding to the three saline water densities are 0.89, 0.81, and 0.74 cm. On this basis l_ρ amounts to 0.81 cm. Also shown in this table is h_w/l_ρ, the ratio of depth of water to the layer thickness. This ratio tends to be more of a constant value, and independent of current velocity. Their average values for $\Delta\rho_s/\rho = 0.02$, 0.04, and 0.06 are 18.8, 21.1, and 22.1. The average is 20.6 as

$$-\frac{h_w}{\Delta\rho_s}\left(\frac{d\Delta\rho}{dz}\right)_{max} = \frac{h_w}{l}, \quad z = 0 \tag{28}$$

and introducing the average value of h_w/l_ρ

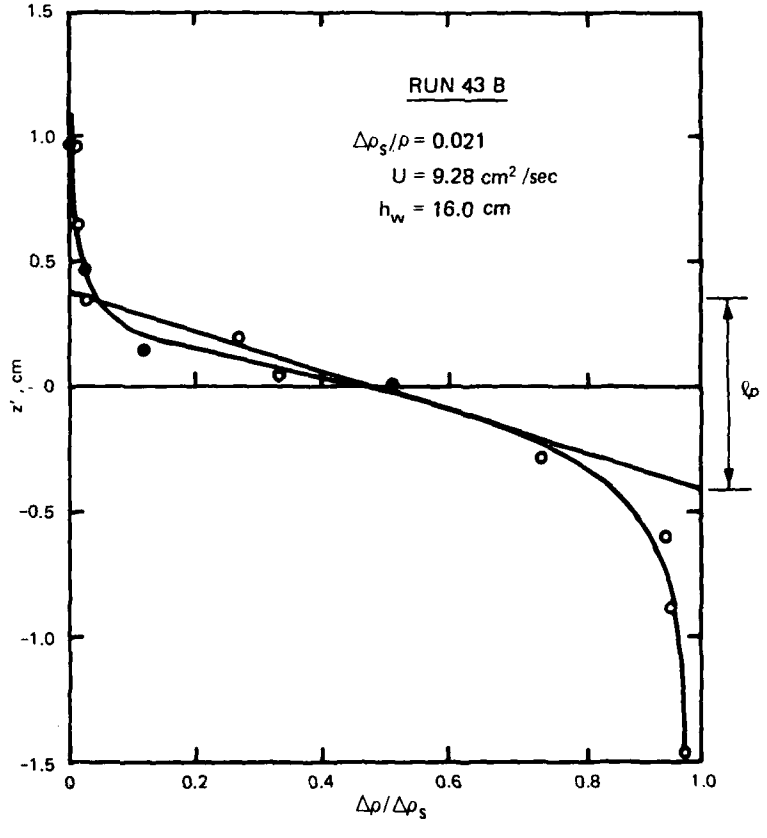

Figure 19. Manner of evaluating interface layer effective thickness on the basis of densities, l_ρ

$$-\frac{h_w}{\Delta\rho_s}\left(\frac{d\Delta\rho}{dz}\right)_{max} = 20.6\ ,\ z = 0 \qquad (29)$$

The determinations of thickness ρ made from the traverses through the cross section $x - 3{,}000$ cm are shown in Table 10. There are slight increases with current velocity. Ignoring these, the average values are $l_\rho = 1.06$, 1.13, and 0.89 corresponding to $\Delta\rho_s/\rho = 0.02$, 0.04, and 0.06, respectively. Thus the average value would be $l_\rho = 1.02$ cm. Here, also, the ratio tends to remain constant for varying current velocity. The average corresponding to $\Delta\rho_s/\rho = 0.02$, 0.04, and 0.06 are 14.3, 12.5, and 16.3, yielding an overall average value

$$\frac{h_w}{l_\rho} = 14.4$$

and thus

$$-\frac{h_w}{\Delta\rho_s}\frac{d\Delta\rho}{dz} = 14.4\ ,\ z = 0 \qquad (30)$$

These results indicate a tendency for l_ρ to increase with distance from entrance. The density measurements in the interfacial region are sparse. Had we selected copper or platinum wires 1/64 in. in thickness for the probe and reduced the spacing between the wires to 2 mm, it would have been possible to observe the densities of the interfacial area at a greater number of points, assuring the certainty of l_ρ values. For an underflow, saline water flowing under a relatively stagnant fresh water, Loftquist (1960) found:

$$\frac{h_r}{l_\rho} = 13.7 \qquad (31)$$

where h_r is the hydraulic radius of saline layer. In his tests h_s/h_r, h_s the depth of saline waters, equals 2.58. This gives

$$\frac{h_s}{l_\rho} = 35.3 \qquad (32)$$

a value about 40 percent larger than the corresponding value noted above for measurements at $x = 2{,}000$ cm.

28. The interfacial layer thickness can be defined also in terms of velocities by the relation

$$\left(\frac{du}{dz}\right)_{max} = \frac{U}{l_u} \tag{33}$$

The graphic determination of l_u is illustrated in Figure 20. Evaluations made for the three saline water relative densities, $\Delta\rho_s/\rho$ = 0.02, 0.04, and 0.06, are shown in Table 11. The values change only slightly with current velocities although there is a tendency for l_u to increase with current velocity. The averages corresponding to three saline water densities are 2.76, 2.48, and 2.66 cm. On this basis l_u amounts to 2.63 cm. Hence thickness based on velocities is twice as large as that based on densities. Also shown in this table is the ratio h_w/l_ρ. Independent of velocity, it tends to a constant value. For $\Delta\rho_s/\rho$ = 0.02, 0.04, and 0.06 the averages are 6.23, 6.78, and 6.22. The overall average is 6.41 yielding

$$\frac{h_w}{U}\frac{du}{dz} = 6.47, \quad z = 0 \tag{34}$$

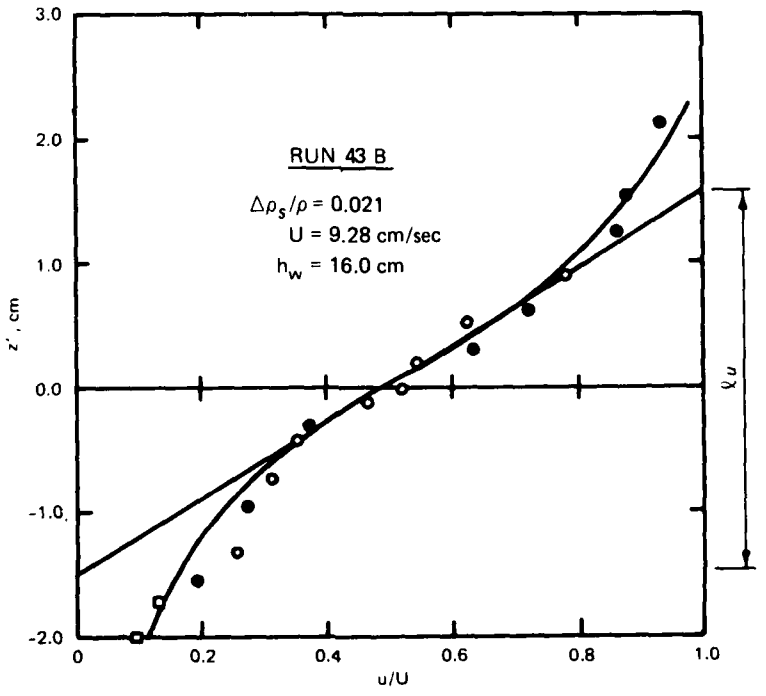

Figure 20. Manner of evaluating interface layer effective thickness on the basis of velocities, l_u

29. Among the earlier investigators, Ellison and Turner (1959) were the first to note that entrainment is related to the gross Richardson number

$$R_i = g \frac{(\Delta\rho_s/\rho)h_w}{U^2} \tag{35}$$

On the other hand, more directly influenced by the mechanism of flow in the interfacial area, entrainment is related to the local Richardson number

$$-R_{io} = \frac{g d\rho/dz}{\rho(\partial u/dz)^2} \ , \ z = 0 \tag{36}$$

The findings of Ellison and Turner would imply that the gross and local Richardson numbers differ from each other by a numerical factor, a point which can be readily demonstrated through the results presented above. Squaring the two sides of Equation 34, dividing the terms of the resulting equation by Equation 29

$$\frac{\Delta\rho_s h_w}{U^2} = -2 \frac{d\rho/dz}{(\partial u/dz)^2}$$

Multiplying both sides by g/ρ

$$\frac{g\Delta\rho_s h_w}{\rho U^2} = -2 \frac{g d\rho/dz}{\rho(du/dz)^2} \tag{37}$$

The numerical factor for the present case is two.

Fresh and Saline Water Densities

30. The pattern of the density distribution in a cross section may be normalized by dividing $\Delta\rho$ by $\Delta\rho_s$ and s the distance from the interface by l_ρ. At the interface $\Delta\rho/\Delta\rho_s$ equals half and l_ρ is the interface effective thickness determined on the basis of densities. This is the procedure used by Loftquist (1960). As an illustration the pattern observed at three cross sections in Run 27 is shown in Figure 21. Density variations are similar to each other in all the sections. The line drawn is according to the relation

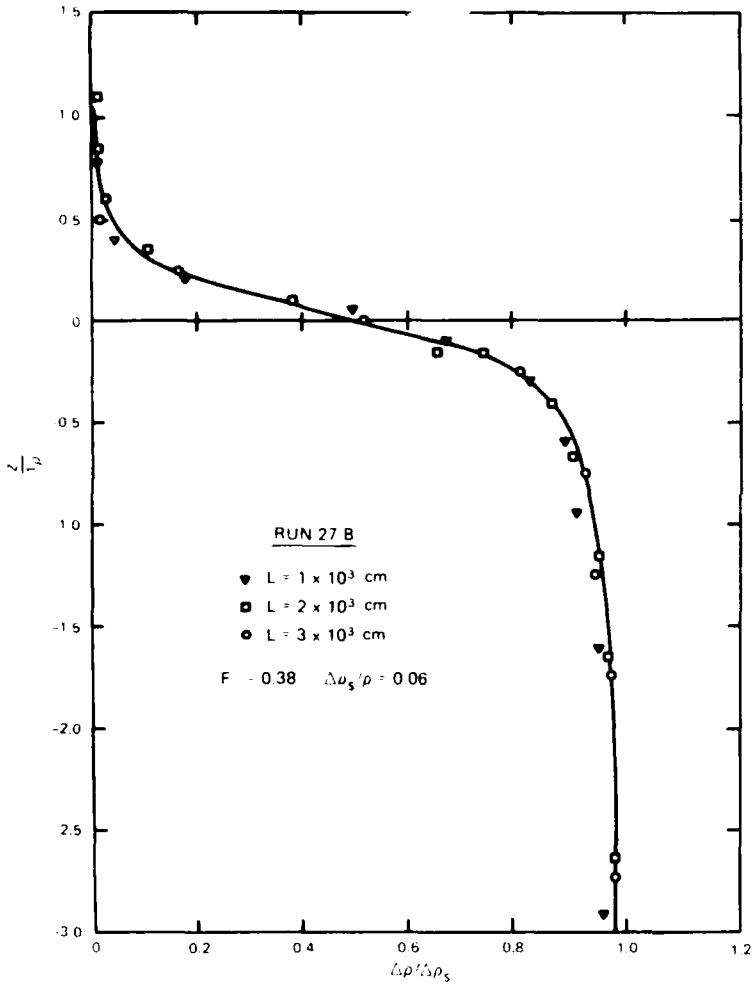

Figure 21. An example of density distribution in three cross sections

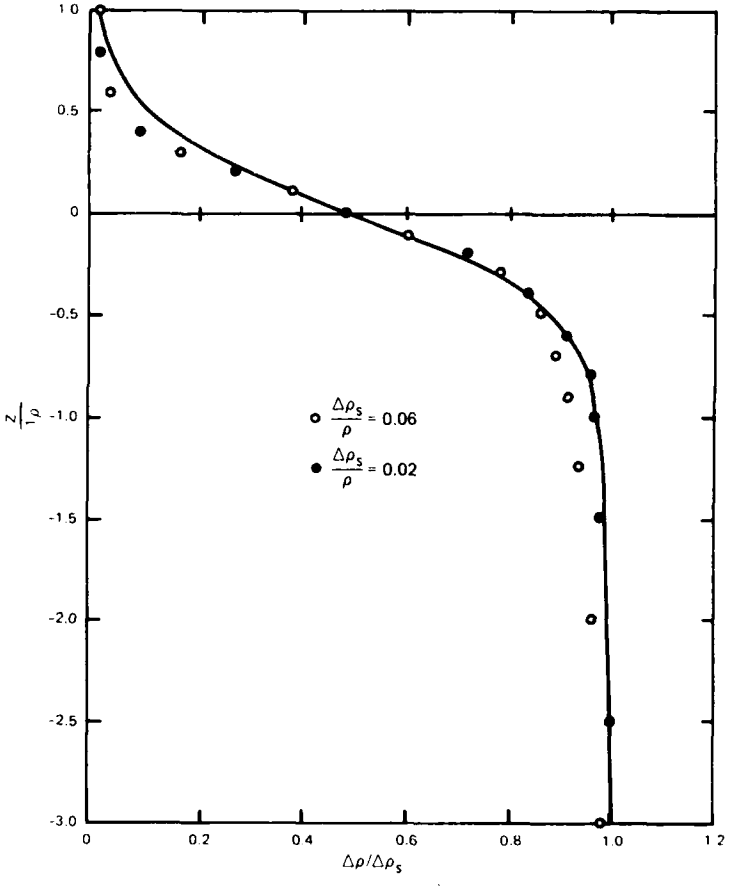

Figure 22. Characteristic density distribution on entire cross section

$$\frac{\Delta\rho}{\Delta\rho_s} = \frac{1}{2}\left(1 - \tanh\frac{2s}{l_\rho}\right) \tag{38}$$

and satisfies the following three conditions: (a) for large values of s/l_ρ positive, $\Delta\rho/\Delta\rho_s$ vanishes; (b) for large values of s/l_ρ negative, $\Delta\rho/\Delta\rho_s$ equals unity; and (c) at $s = 0$, $(d/ds)(\Delta\rho/\Delta\rho_s) = 1/l_\rho$. It is noticed further that in the observations made at a selected cross section the pattern of densities is practically independent of the density of saline water and the densimetric Froude number of the flow. Thus the data manifesting only slight variations between them may be averaged. The summarized values for the two cross sections $x = 2{,}000$ cm and $x = 3{,}000$ cm are shown in Figure 22. The line drawn is also in accordance with Equation 38. The agreement of the saline values with the curve is quite satisfactory. On the other hand, for the fresh water a marked disparity from the curve is very noticeable.

31. The range of densimetric Froude number encountered in this study is 0.1 to 0.5. When the densimetric Froude number is less than 0.28, $\Delta\rho/\Delta\rho_s$ of the freshwater area above the interfacial layer nearly vanishes. There is no transport of salt into fresh water. On the other hand, when F_Δ is greater than this value the salt transport is of significant amount and furthermore it increases with distance from the entrance. In a given section $\Delta\rho/\Delta\rho_s$ is inversely proportional to distance measured from the interface line. Proportionality factor changes with cross section as illustrated in Figure 23. It is convenient toward the formulation to introduce the coefficient β defined as

$$\frac{\Delta\rho_s}{\Delta\rho} = \frac{\beta z}{h_w} \tag{39}$$

The plotting in Figure 24 leads to

$$\frac{\beta L}{h_w} = 4 \times 10^3 F_\Delta^{-4} \tag{40}$$

and that in Figure 25

$$\frac{\beta L}{h_w} = 6.0 \times 10^{13} R^{-2} \tag{41}$$

There is considerable scattering of data points in both figures due mainly to the difficulty in the graphic determination of β.

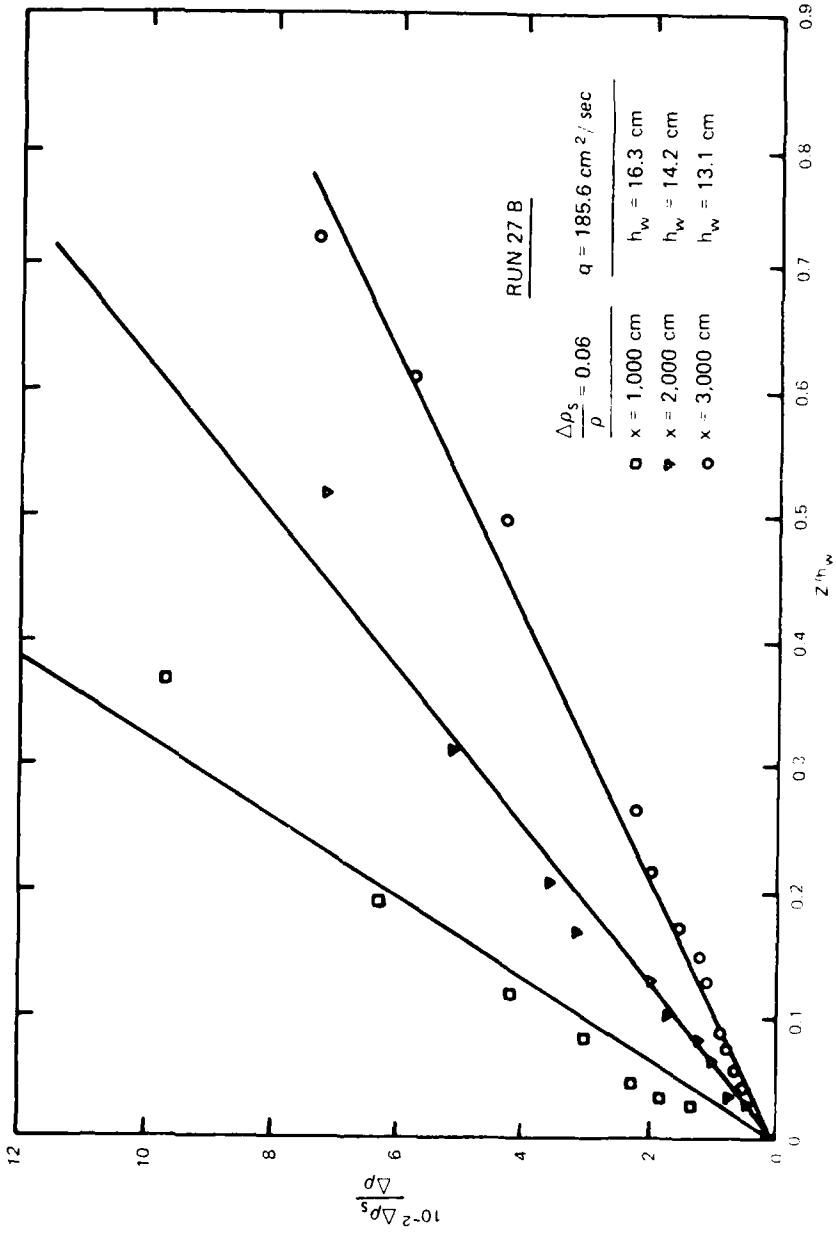

Figure 23. An example of density distribution in freshwater layer at three stations

Partial Entrainment Ratio U_{m1}/U

40. The transport velocity U_{m1} may be expressed also as

$$U_{m1} = \frac{Q_{s1}}{L} \tag{63}$$

where

$$Q_{s1} = U \int_{-\delta_o}^{l_\rho/2} \frac{\Delta\rho}{\Delta\rho_s} \frac{u}{U} \, dz \tag{64}$$

The quantity $x\Delta\rho_s Q_{s1}$ represents the mass of salt transported by the interface layer. The lower limit is identified as the depression of the point where the relative density $\Delta\rho/\Delta\rho_s$ equals 0.99 as measured from the interfacial line $z' = 0$. Considerable difficulty is experienced in deciding just what the exact value of δ_o is. This, however, is not a serious matter since at this point u/U is small. Nevertheless, it is a source of some error. As regards the upper limit $l_\rho/2$, it will be remembered that it changes slightly with the fresh current velocity and also with length L. For convenience, however, $l_\rho/2$ is taken to equal 0.01 ft. The question whether Q_{s1} varies linearly with or is a constant independent of L cannot be answered with certainty. Now, one may write

$$\frac{Q_{s1}}{U} = \frac{m}{2} \frac{u_i}{2} l_\rho \tag{65}$$

This expression, with Q_{s1} evaluated on the basis of Equation 64 and l_ρ from observed data, allows the determination of m. Results from the runs for the three saline waters are shown in the following set of values where m_2 and m_3 relate to observations made at the cross sections $x_2 = 2{,}000$ cm and $x_3 = 3{,}000$ cm, respectively.

$\Delta\rho_s/\rho$	$l_{\rho 2}$, cm	m_2	$l_{\rho 3}$, cm	m_3
0.02	0.89	1.26	1.12	1.49
0.04	0.80	1.17	1.17	1.81
0.06	0.78	1.13	1.13	1.79

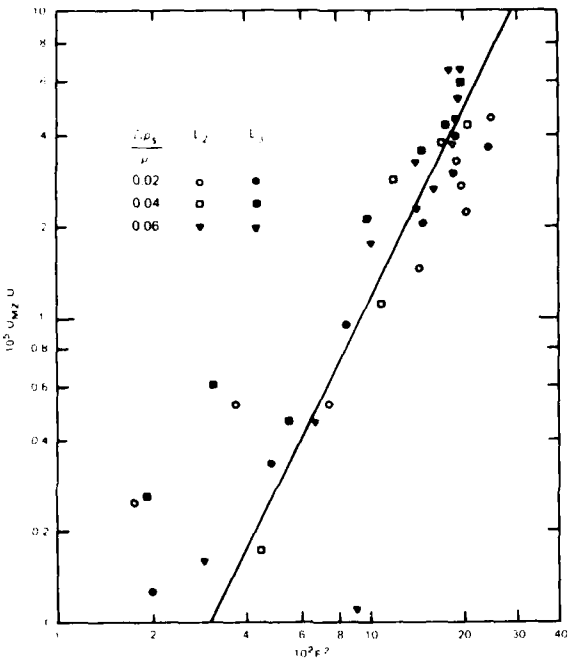

Figure 31. Coefficient of saline water transport into fresh water against densimetric Froude number

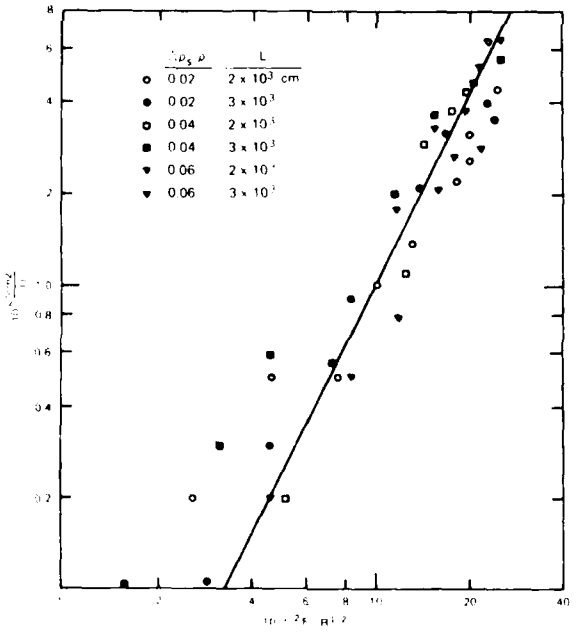

Figure 32. Coefficient of saline water transport into fresh water against a combined parameter

$$U_c = \kappa_1 \left(\frac{\nu g \Delta\rho_s}{\rho} \right)^{1/3} \tag{59}$$

which may be written also as

$$U_c = \kappa_2 \left[(F_{\Delta c})^2 \cdot R_c \right]^{1/3} \tag{60}$$

Utilizing the above noted set of values, Equations 59 and 60 yield separately

$\Delta\rho_s/\rho$	κ_1	κ_2
0.02	8.75	8.75
0.04	9.28	8.67
0.06	9.16	8.62

Below densimetric Froude number 0.28, $\Delta\rho/\Delta\rho_s$ vanishes in fresh water above the interfacial layer. The condition of densities for densimetric Froude number larger than 0.28 was previously discussed.

39. Taking the values of U_{m2}/U from Tables 20, 21, and 22 relating to saline waters of relative densities, $\Delta\rho_s/\rho$ = 0.02, 0.04, and 0.06, respectively. These are plotted against $10^2 F_\Delta^2$ in Figure 31. The equation of the line drawn is

$$\frac{U_{m2}}{U} = 0.034 F_\Delta^4 \tag{61}$$

applicable in the range of F_Δ from 0.28 to 0.55. The scatter of the points in the region inferior to 0.28 may be attributed to the fact that the transport from the interface layer into fresh water, as mentioned above, is exceedingly small and their values are irregular and cannot be determined accurately. Another presentation is given in Figure 32, where the equation of the line drawn is

$$\frac{U_{m2}}{U} = 0.31 \times 10^{-6} F_\Delta^2 R \tag{62}$$

In the latter presentation, points are more closely placed to the curve drawn. Which of the two relations for U_{m2}/U is valid actually is a question that cannot be ascertained in the present study. In the tests made, as mentioned previously, R and F_Δ are nearly related to each other.

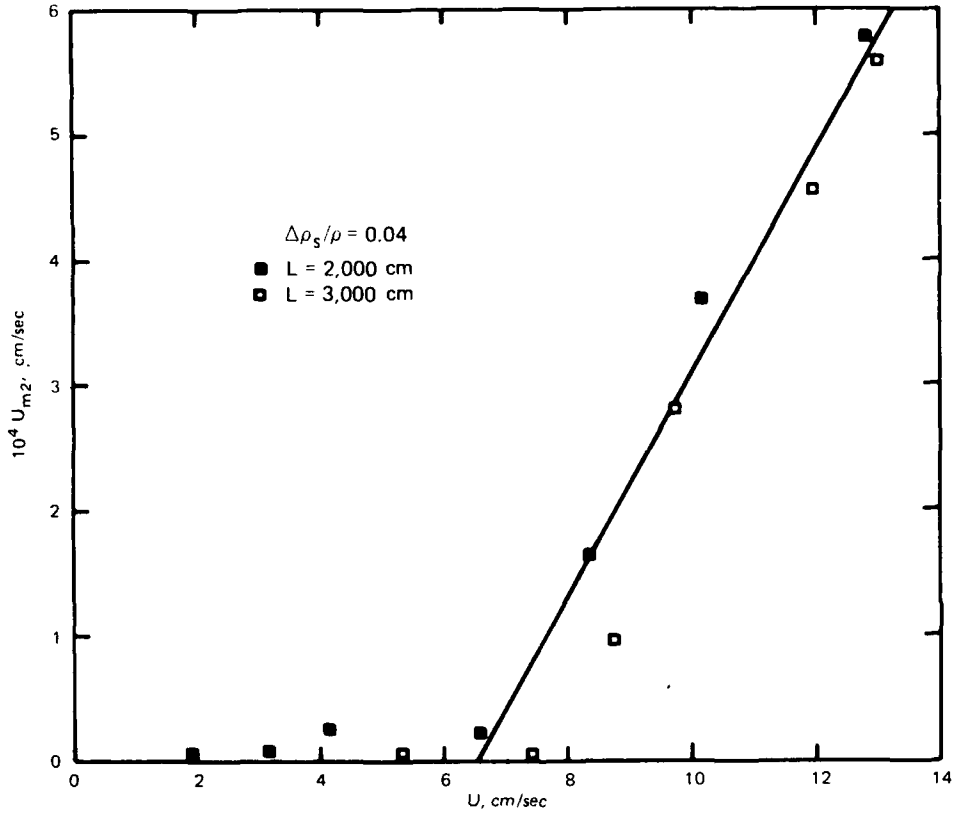

Figure 30. Freshwater component of saline water transport against current velocity

$\Delta\rho_s/\rho$	$10^{-2}\nu$	$10^2(F_\Delta)^2_c$	$10^{-3}R_c$	$10^{-1}(F_{\Delta c})^2 R_c$	U_c
0.02	0.91	8.5	8.0	68	4.90
0.04	1.06	8.0	10.0	80	6.50
0.06	1.00	7.0	11.0	77	7.30

If it be assumed that the critical velocity be independent of water depths, h_s or h_w,

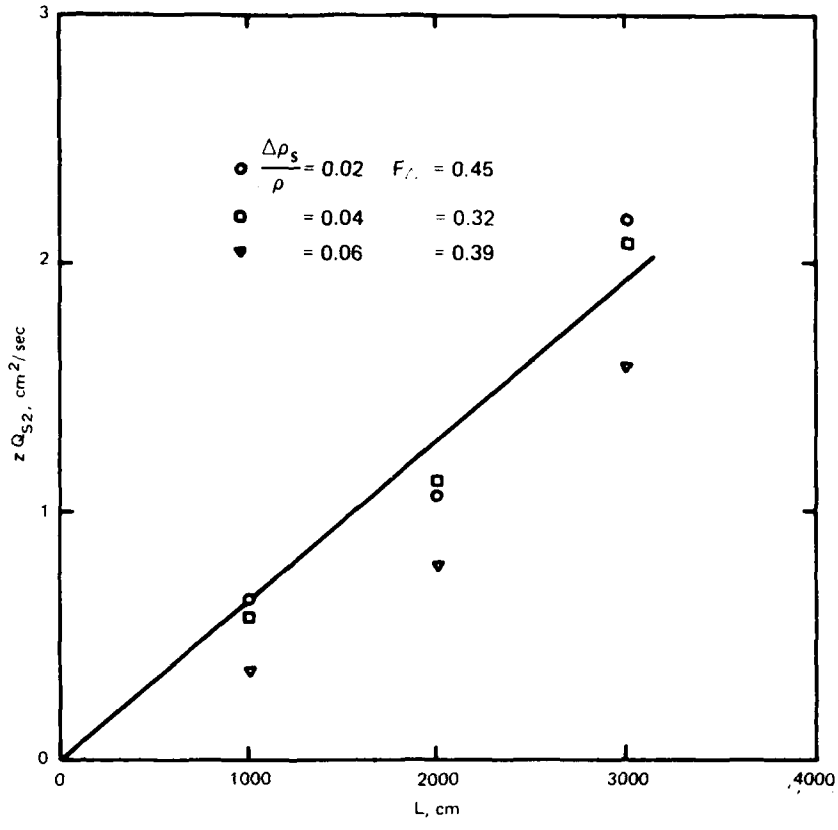

Figure 29. Volume of saline water entering into current from the interface layer

is shown in Tables 17, 18, and 19, respectively. The quantities h_w and U appearing in these tables represent the average values of depth and current velocities over the length L.

38. In Figure 30, as an illustration, we have plotted U_{m2} against U for the case of $\Delta\rho_s/\rho = 0.04$, taking values from Table 18. Two facts may be readily deduced. First, the data from two cross sections are in close agreement with each other. Secondly, U_{m2} is practically nil below a critical velocity U_c. The latter fact signifies that no saline water from the interface layer enters into the flowing fresh water below the critical. One may associate with the latter a critical densimetric Froude number $(F_\Delta)_c$ or a critical Reynolds number $(R)_c$ and which may be determined by plotting U_{m2} against F_Δ or against R. Examination yields the following set of values:

$$\int_{x_1}^{x_2} y\, dx$$

Imagine that the interval x_1 to x_2 is divided into equal segments of a common value Δx and the ordinate values y_1, $y_2 \cdots y_{n-1}$, y_n are noted. Granting that Δx is small, y varies linearly in segment Δx.

$$\int_{x_1}^{x_2} y\, dx = \sum_{i=1}^{i=n} y_i - \frac{1}{2}(y_1 + y_n) \tag{57}$$

In accordance with this, the integration in Equation 56 may be replaced by the summations

$$Q_{s2} = U \Sigma \left(\frac{\Delta\rho}{\Delta\rho} \frac{u}{U}\right) dz_1 + U \Sigma \left(\frac{\Delta\rho}{\Delta\rho_s} \frac{u}{U}\right) dz_2 \tag{58}$$

For the evaluations carried out, dz_1 is taken equal to 0.01 in the first summation covering the interval from $z' = 0.01$ to $z' = 0.1$ ft; in the second summation, dz_2 is taken equal to 0.15 ft covering the interval $z' = 0.1$ to $z' = h_w$ ft. For a given z', $\Delta\rho/\Delta\rho_s$ is read from curves similar to those shown in Figure 28. The corresponding u/U value is read from the curve shown in Figure 14 after z'/h_w ratio is formed. The Q_{s2} values thus computed are shown in Table 16 and these are plotted in Figure 29. Distribution of the plotted points admits a linear alignment, practically, showing that U_{m2} is uniform.

Partial Entrainment Ratio U_{m2}/U

37. The observations of $\Delta\rho/\Delta\rho_s$ in the main are made at two cross sections $x_2 = 2{,}000$ cm and $x_3 = 3{,}000$ cm. In every instance U_{m2} is established first evaluating Q_{s2} in the manner explained above and then dividing it by the interfacial length L corresponding to the cross section where the density determinations are made. The entire list of the results covering the saline water relative densities $\Delta\rho_s/\rho = 0.02$, 0.04, and 0.06

illustration, the case of $\Delta\rho_s/\rho = 0.06$ and $q = 185.6$ cm^2/sec is selected. The relative density values in the three cross sections are shown in Tables 13, 14, and 15; these are plotted in Figure 28. To avoid the confusion of plotted points, two of the graphs are displaced downward. The relative position of the curves indicates that the transport of salt increases with distance from the entrance.

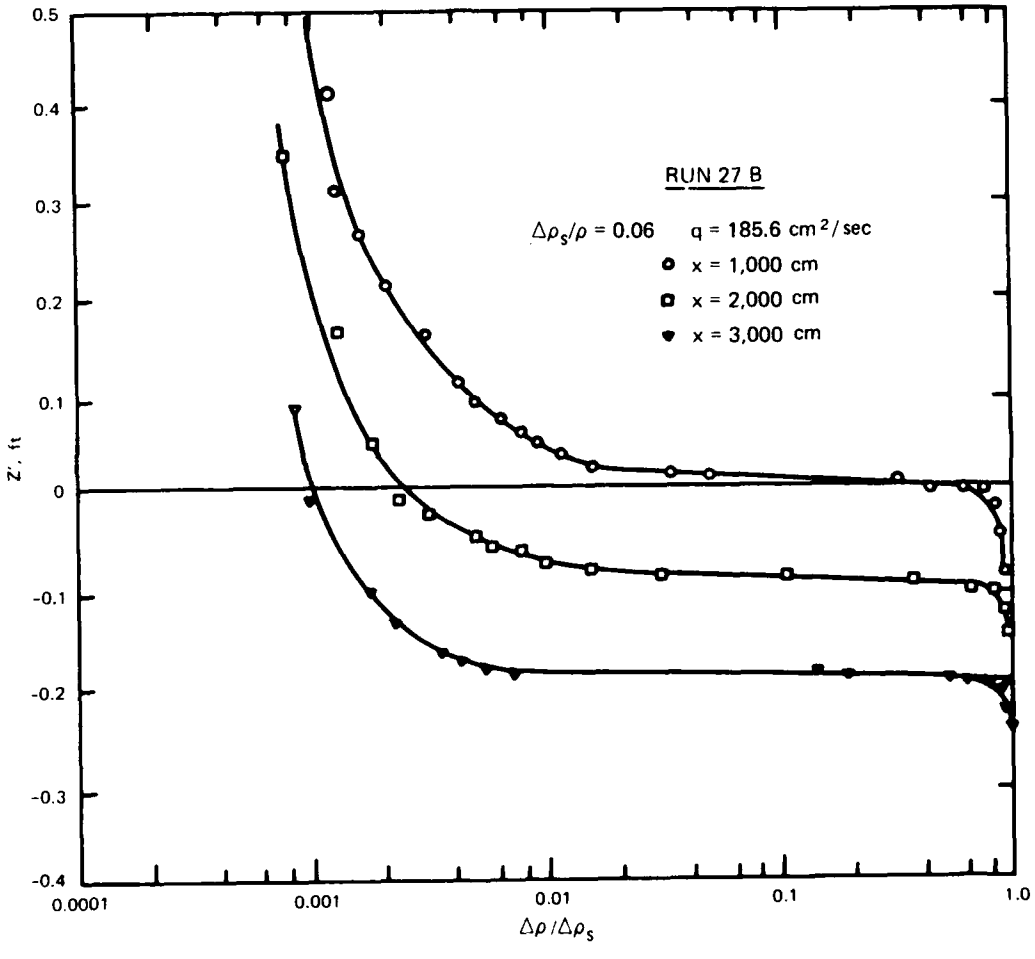

Figure 28. An example of density distribution in freshwater layer

36. An integration in subsequent evaluations is replaced by a summation. Consider the integral

Local velocity u is normalized by expressing it in terms of the mean velocity of current, $U = q/h_w$. The analysis of entrainment will be carried out in two steps by considering separately the transport of salt in the interface layer and the fresh water above the interface layer. Toward this end

$$U_m = U_{m1} + U_{m2} \tag{52}$$

$$U_{m1} = \frac{U}{L} \int_{-\delta_o}^{l_\rho/2} \frac{\Delta\rho}{\Delta\rho_s} \frac{u}{U} \, dz' \tag{53}$$

and

$$U_{m2} = \frac{U}{L} \int_{l_\rho/2}^{h_w} \frac{\Delta\rho}{\Delta\rho_s} \frac{u}{U} \, dz' \tag{54}$$

where U_{m1} relates to salt transport into the interface layer and U_{m2} to that into fresh water above the interface.

Uniformity of Saline Transport Velocity U_{m2}

35. The transport velocity U_{m2} may be expressed also as

$$U_{m2} = \frac{Q_{s2}}{L} \tag{55}$$

where

$$Q_{s2} = U \int_{l_\rho/2}^{h_w} \frac{\Delta\rho}{\Delta\rho_s} \frac{u}{U} \, dz' \tag{56}$$

The quantity $\alpha\Delta\rho_s Q_{s2}$ represents the mass of salt transported per second by the part of fresh water lying above the interface layer upper limit $z = l_\rho/2$. If one finds that Q_{s2} varies linearly with L, then this will indicate that entrainment velocity U_{m2} is uniform. The matter can be examined for larger freshwater discharge considering the $\Delta\rho/\Delta\rho_s$ values for the three cross sections at x = 1,000, 2,000, and 3,000 cm. As an

increase in the value of α when the solution is dilute. For the present, we will take α to have the constant value 1.60 also in dilute solutions.

34. Density of the saline water is $\rho + \Delta\rho_s$ and U_m is the velocity of entrainment, then the mass of salt transported across the interface of length L would be

$$\int_0^L \alpha\Delta\rho_s U_m \, dx$$

Again, on the same basis, the mass of salt transported by the fresh water across the cross section at $x - L$ would be

$$\int_{-\delta_o}^{h_w} \alpha\Delta\rho u \, dz'$$

The distance z' is measured from the interface line where $\Delta\rho/\Delta\rho_s = 1/2$. The velocity and density of fluid passing the point z' are u and $\rho + \Delta\rho$, respectively. The upper limit h_w represents the elevation of the free surface from the interface line and the lower limit δ_o represents the depression of the point where $\Delta\rho/\Delta\rho_s$ equals 0.99. The determination of δ_o is open to error, and it may be inferred from Figure 22 that δ_o is of the order

$$\delta_o = 21_\rho \tag{49}$$

Since water initially traversing the cross section at $x = 0$ is devoid of salt, the conservation of mass requires that

$$\int_0^L \alpha\Delta\rho_s U_m \, dx = \int_{-\delta_o}^{h_w} \alpha\Delta\rho u \, dz' \tag{50}$$

Assuming that U_m is uniform along the interface, α is of constant value, the above yields

$$U_m = \frac{U}{L} \int_{-\delta_o}^{h_w} \frac{\Delta\rho}{\Delta\rho_s} \frac{u}{U} \, dz' \tag{51}$$

PART IV: SALINE ENTRAINMENT INTO FRESH WATER

Formula of Entrainment

33. The transport of saline water through the interface will be determined on the basis of the transport of salt by fresh water in a cross section. Let a solute of mass M and of density ρ_m be dissolved in a pure water of volume Ω. Let Ω_s and $\rho + \Delta\rho$ denote the volume and the density, respectively, of the resulting solution, ρ being the density of water. Denoting the volume of the solute by Ω_m, the mass of solute is $\rho_m\Omega_m$. As the mass of the solution is equal to the sum of the masses of the components

$$(\rho + \Delta\rho)\Omega_s = \rho_m\Omega_m + \rho\Omega \tag{44}$$

The corresponding relation for the volume would be

$$\Omega_s = \Omega + \varepsilon\Omega_m \tag{45}$$

where ε is a factor to be determined. From Equations 44 and 45 we obtain

$$\rho_m\Omega_m = \alpha\Delta\rho\Omega_s \tag{46}$$

where

$$\alpha = \left(1 - \varepsilon\frac{\rho}{\rho_m}\right)^{-1} \tag{47}$$

The relation of α to salinity S would be

$$S\left(1 + \frac{\Delta\rho}{\rho}\right) = \alpha\frac{\Delta\rho}{\rho} \tag{48}$$

Usually S is defined as a ratio expressing the number of grams of salt per kilogram of saline solution. In Table 12, the relation between α and $\Delta\rho/\rho$ is shown. For larger salinities α may be taken as 1.51. In more dilute solutions α increases according to this tabulation. Meanwhile, for $S = 0.01$, the corresponding value of ε is 1.032, a number greater than unity. This is not very likely to happen and therefore we question the

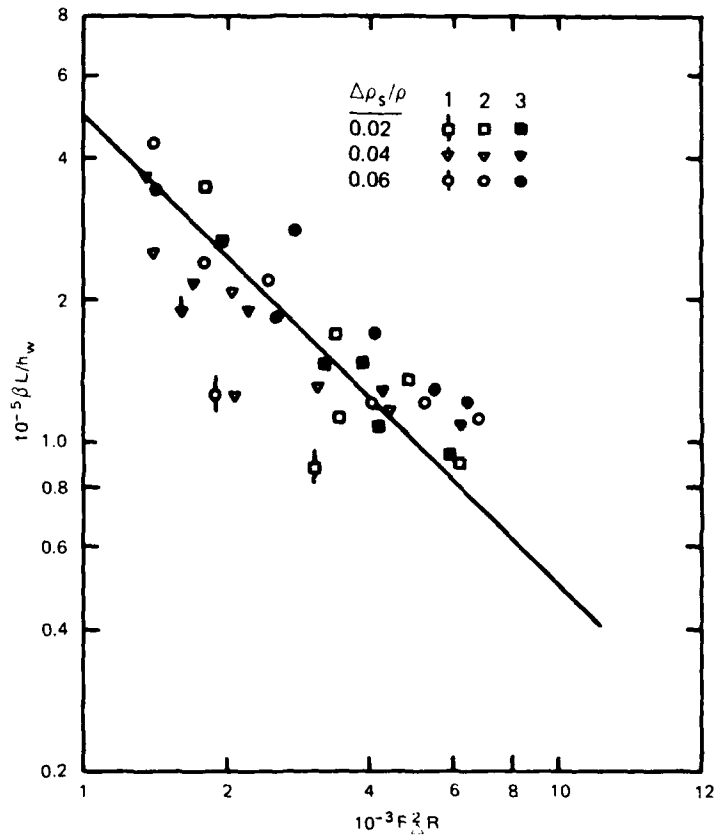

Figure 27. Dependence of coefficient of β on a new number $F_\Delta^2 R$

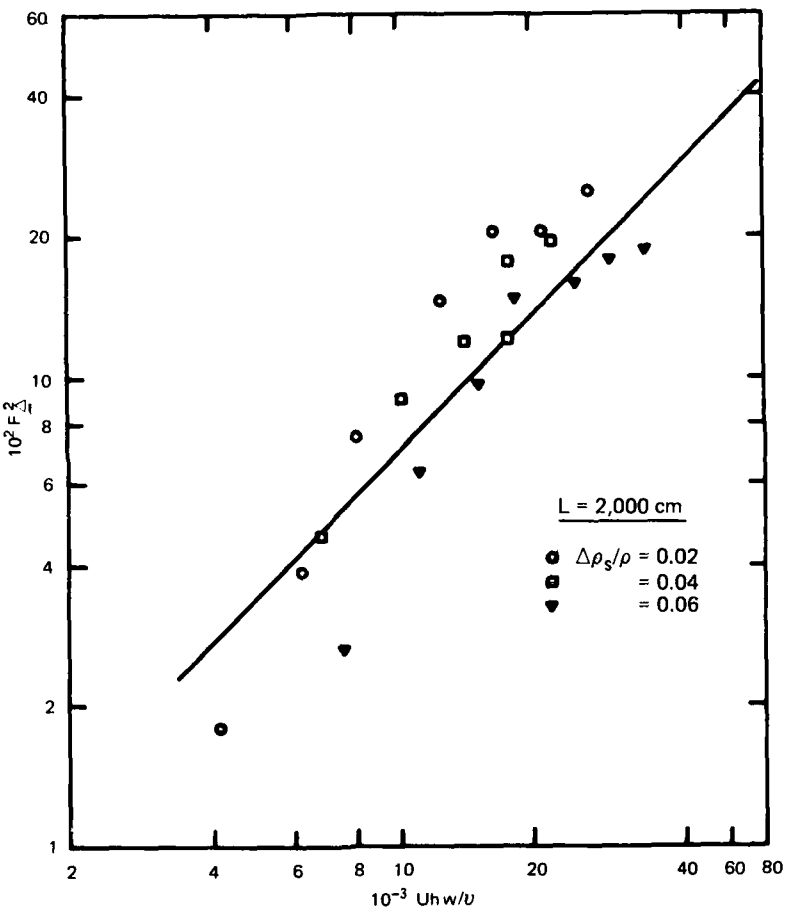

Figure 26. Relationship between Reynolds number and densimetric Froude number in tests

32. Here we encounter a difficult situation as $\beta L/h_w$ may be expressed as a function either of densimetric Froude number or of Reynolds number. This may be brought about if because of limited range of quantities employed during the tests there is a definite relationship between the Reynolds number and the densimetric Froude number encountered. In Figure 26, the F_Δ^2 and R values noted during the measurements at the cross section $x = 2{,}000$ cm are shown. Equations 39 and 40 imply that

$$10^2 F_\Delta^2 = 0.82\ (10^{-3} R) \tag{42}$$

and the curve drawn through the larger F_Δ values is in accordance with this relation. There is also a third possibility of representation. Again, on the basis of Equation 40 and Equation 41 we also have

$$\frac{\beta L}{h_w} = 4.88\ 10^8 F_\Delta^{-2} R^{-1} \tag{43}$$

The observed values of $\beta L/h_w$ are plotted against $F_\Delta^2 R$ in Figure 27. In the latter figure, the dispersion of data points is less severe than those in Figures 25 and 26. Hence, Equation 43 is a more valid relation for $\beta L/h_w$. Apparently it will be difficult in density current research to evaluate exactly the role of densimetric Froude number or Reynolds number on a particular item if the magnitude of the physical quantities involved fall in a small range.

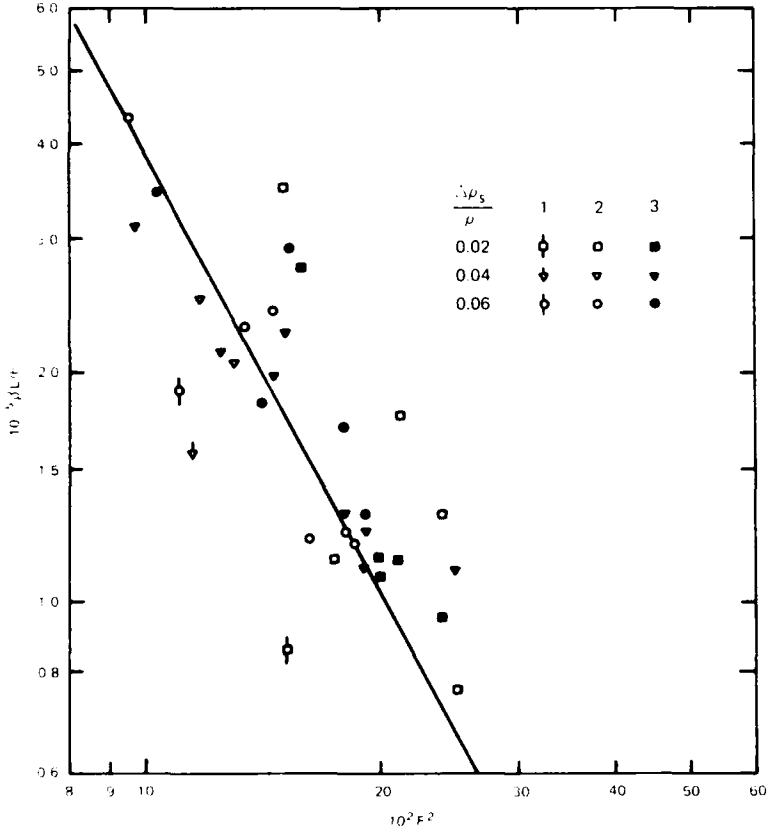

Figure 24. Dependence of coefficient β on densimetric Froude number

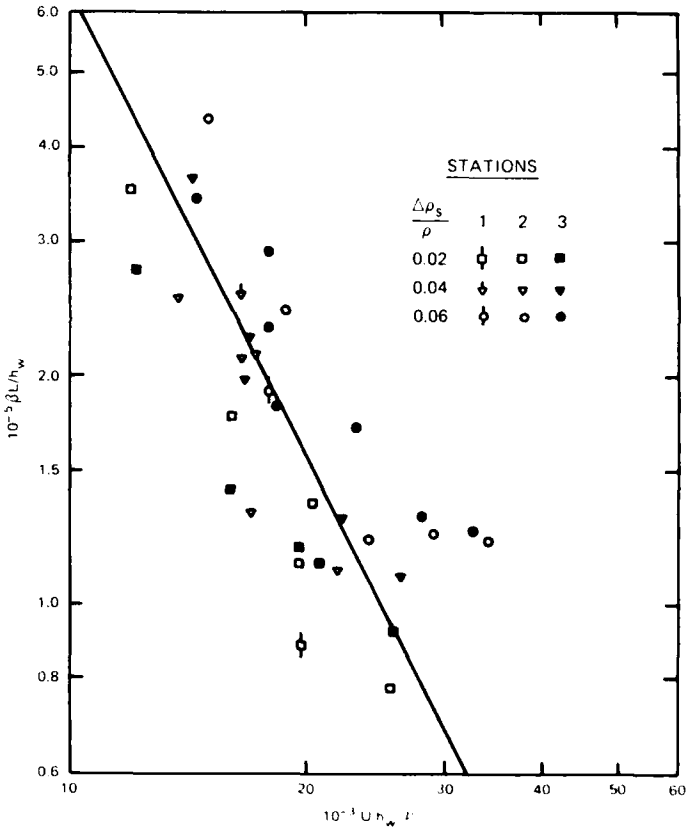

Figure 25. Dependence of coefficient β on Reynolds number

On the basis of averages of the items above

$$\frac{ml_{\rho}}{L_2} = 0.67$$
$$\frac{ml_{\rho}}{L_3} = 0.54 \qquad (66)$$

indicating that Q_{sl} is almost proportional to L, at least in the area of L_2 to L_3. We now assume that this proportionality is valid for the area $x = 0$ to $x = L$. The values of U_1/U computed using Equations 63 and 64 are shown in the Tables 17, 18, and 19 for the saline waters of relative densities $\Delta\rho/\rho = 0.02$, 0.04, and 0.06, respectively. These are next plotted versus F_{Δ}^2 in Figure 33. The ratio U_{ml}/U varies but little with the

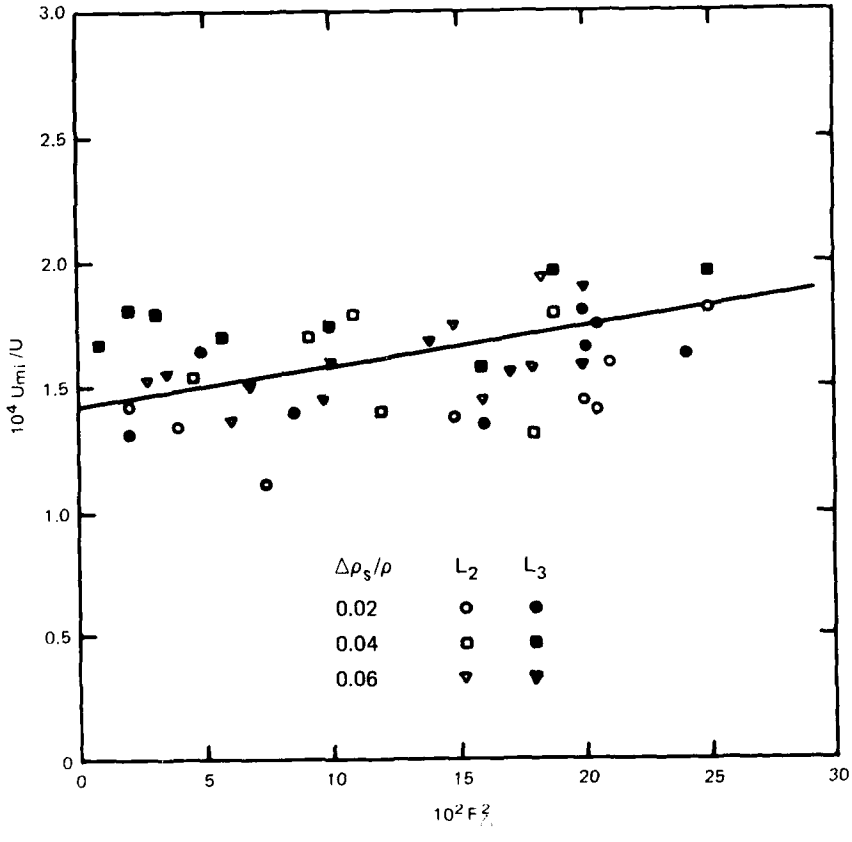

Figure 33. Coefficient of saline water transport relative to interface layer versus densimetric Froude number

densimetric Froude number. The line drawn in the figure yields the relation

$$\frac{U_{m1}}{U} = 1.5 \times 10^{-4} \ (1 + 1.1 \ F_{\Delta}^2) \qquad (67)$$

Entrainment Ratio U_m/U

41. The entrainment ratio U_m/U is the sum of the partial entrainment ratios U_{m1}/U and U_{m2}/U. The computed values from the observations are shown in Tables 20, 21, and 22 for the saline water densities $\Delta\rho_s/\rho = 0.02$, 0.04, and 0.06. These are next plotted versus F_{Δ}^2 in Figure 34. Although

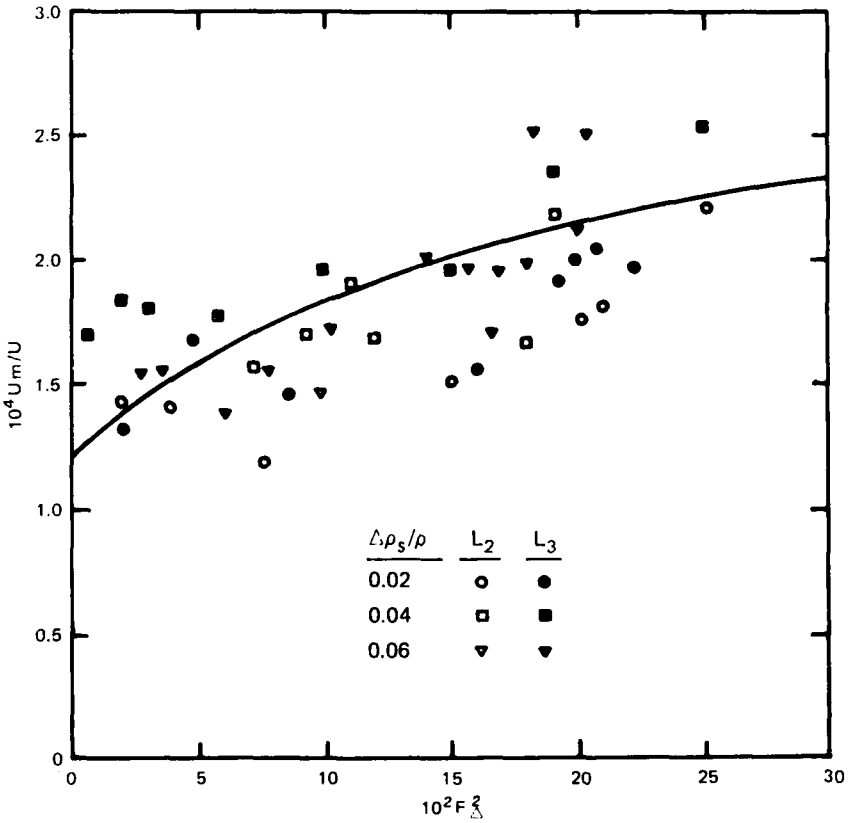

Figure 34. Dependence of entrainment ratio upon densimetric Froude number

the distribution of points suggests a linear alignment, preferring a power formula, a curve is drawn in accordance with

$$\frac{U_m}{U} = 3 \times 10^{-4} F_\Delta^{2/5} \tag{68}$$

Suga (1975) gives the formula

$$\frac{U_m}{U} = 6 \times 10^{-3} F_\Delta^{10/3} \tag{69}$$

deduced from experiments on arrested wedges carried out in a channel of 100-m length and 80-cm width and with saline waters in the range of $\Delta\rho_s/\rho = 0.005$ to 0.03 . Here U denotes the river velocity at the tip of wedge and F_Δ is based on the velocity of river and water depth at the tip of wedge. The range of river depth is 40 to 80 cm and the discharge, q , 10 to 600 cm^2/sec. Both formulas give like values of U_m/U at $F_\Delta^2 = 15$; at $F_\Delta^2 = 5$, Suga formula gives a value four times smaller and at $F_\Delta^2 = 30$, four times greater than the ones from Equation 67.

42. The disparity between the evaluation from Equations 68 and 69 is a matter of much puzzlement. It will be recalled that the results of the present study on entrainment are based on the density traverses at two cross sections $x_2 = 2{,}000$ and $x_3 = 3{,}000$ cm, assuming that velocity of entrainment U_m for a given water discharge is uniform and constant across the entire length of the interface. Ellison and Turner (1959) referring to test conditions relating to surface jets over saline waters state: "Mixing began as before, but the rate of increase of depth soon became smaller and at a certain distance downstream, depending on the density difference and the rate of flow, the 'jet' region changed smoothly to one where depth changed little with distance. The turbulence in the mixed layer was damped and there was no further mixing with the salt solution below; the layer then remained of constant depth until it reached the second weir." In this study, significantly the interface layer gradually became more turbulent with distance, noted during the velocity measurement of the interface by globules.

43. In the Ellison and Turner study, mixing between saline and fresh waters is confined to a small region next to flow entrance. Anwar and Weller (1981) give additional information and in particular regarding the dimensions of the area. Freshwater depth increases linearly with distance

from the entrance. Denoting the depth of fresh water at the entrance by h_o and the length of the mixing zone by x, the ratio x/h_o increases with the densimetric Froude number F_Δ, $x/h_o < 3$ when $F_\Delta = 0.7$, $x/h_o = 10$ when $F_\Delta = 1.85$. When F_Δ equals 0.52 the entrainment zone almost disappears. The maximum F_Δ met with the present study is always less than 0.5, and if the Anwar and Weller findings remain applicable, then mixing zones at the flow entrances should be absent. The measurement of the saline water heights h_s in this present study commences with the cross section at $x = 133$ cm. Downstream of this cross section, the depth of fresh water h_w continually increases. The condition of the interface upstream of this initial cross section is not studied; it may be assumed that in this area the interface remains practically horizontal such as shown in Figure 35.

44. Anwar and Weller using data from various investigations in addition to their findings give the form

$$\frac{U_m}{U} = 4.5 \times 10^{-3} F_\Delta^3 \qquad (70)$$

for large values of F_Δ. This is sufficiently close to the form proposed by Suga. Results from Loftquist (1960) have been considered. The Loftquist results, however, relate to an underflow and the experiments were carried out in the same channel as the present investigation. An important point to note is that Loftquist in arriving at a value of U_m/U takes U_m to be uniform all along the entire interface. Then it is very surprising to find that U_m/U values would agree with each other whether the determinations are made from a short area of the interface or from the entire interfacial area.

45. Probably the deviation of U_m/U values of the present investigation from those of other investigations is related to the end conditions of the experimental environment channel geometry of the entrance segment as shown in Figure 1. If Huppert and Britter (1982) criteria for flow separation are applied to the present test conditions, since the flows are subcritical on the two sides of the inclined entrance, a separation of flow over saline waters is expected. The resulting flow pattern could not be conducive to mixing. Note also the unusual manner in which the fresh water is removed from the exit segment shown in Figure 2. Theoretically, this matter is important and it may be desirable to reexamine mixing characteristics of a channel where the two ends have inclined bottoms and the flow out is over a weir.

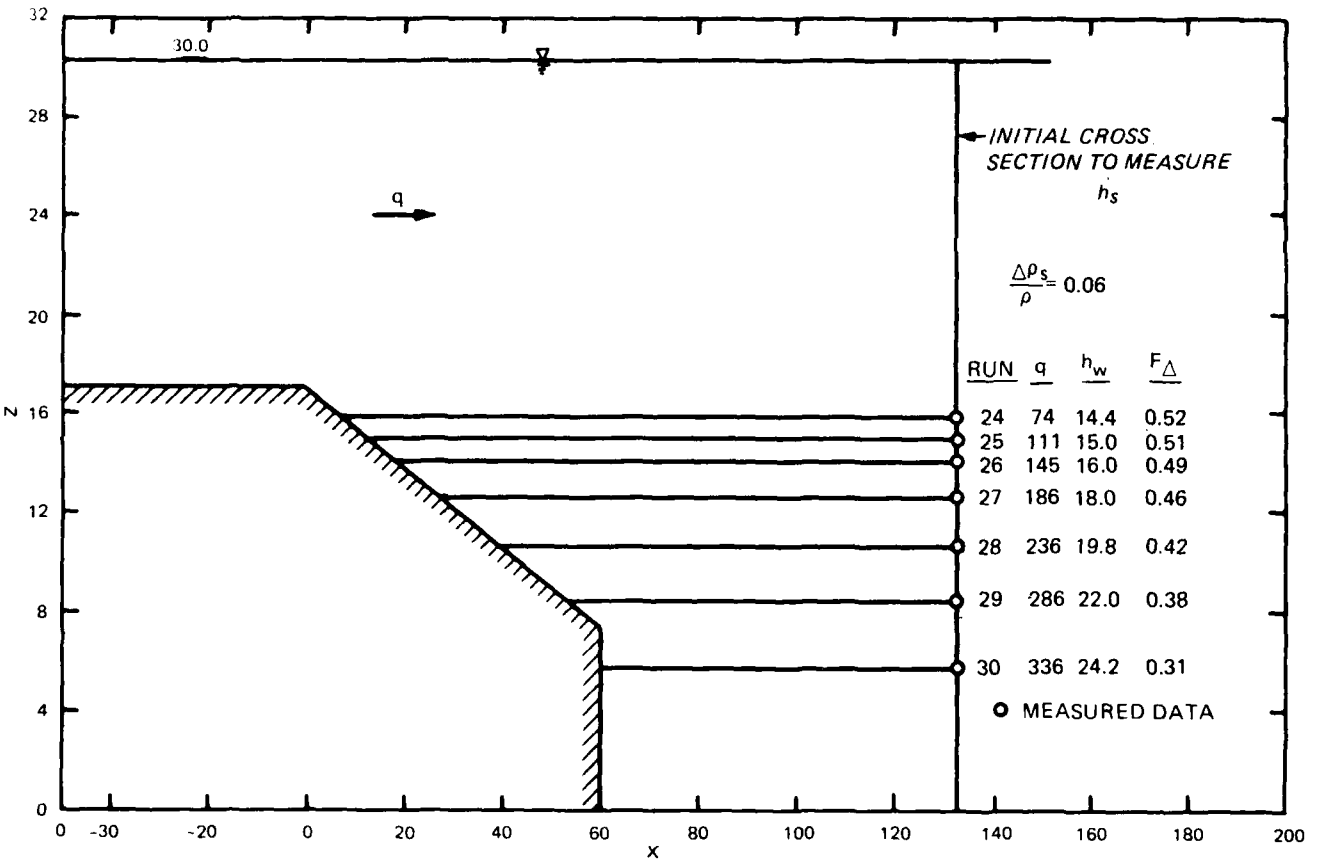

Figure 35. Saline water interface elevation of channel entrance segment

PART V: INTERFACIAL AND BOTTOM STRESSES

Hydrodynamics of Freshwater Layer

46. Let the x-axis be drawn in the direction of the freshwater flow, z-axis vertically upward, and y-axis laterally with the limits -b and b. Let B, H, h_w, and h_s denote the width of channel, the liquid total depth, depth of fresh water, and depth of saline water, respectively. The velocity components along x, y, and z are u, v, and w, respectively (Figure 36). Ignoring the turbulent stresses $-\rho\ \overline{u'u'}$ and $-\rho\ \overline{w'w'}$

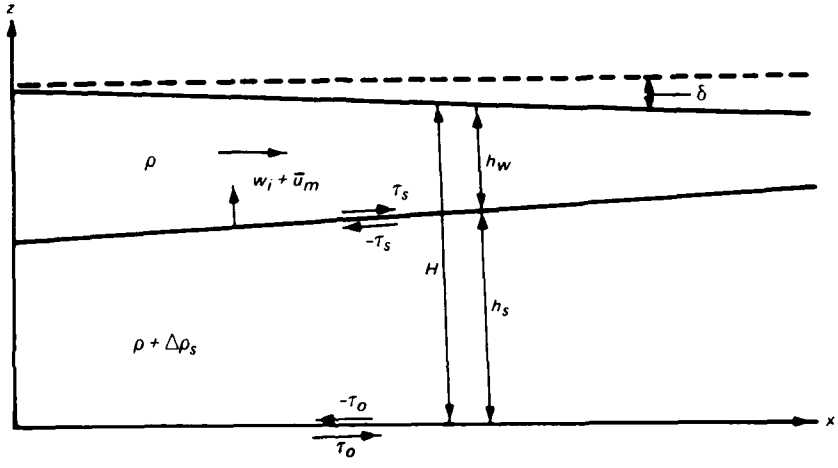

Figure 36. Notation diagram of layer quantities

in comparing with the pressure p and utilizing the condition of continuity, neglecting v,

$$\frac{\partial u}{\partial x} + \frac{\partial w}{\partial z} = 0 \tag{71}$$

and the equations of motion in terms of Lamb's notation are

$$\frac{\partial u^2}{\partial x} + \frac{\partial}{\partial z}(uw) = \frac{1}{\rho}\frac{\partial p}{\partial x} + \frac{1}{\rho}\frac{\partial p_{yx}}{\partial y} + \frac{1}{\rho}\frac{\partial p_{zx}}{\partial z} \tag{72}$$

$$u^2\frac{\partial}{\partial x}\left(\frac{w}{u}\right) = -g - \frac{1}{\rho}\frac{\partial p}{\partial z} + \frac{1}{\rho}\frac{\partial p_{xz}}{\partial x} + \frac{1}{\rho}\frac{\partial p_{yz}}{\partial y} \tag{73}$$

ρ being the density of fresh water. Here, p_{yx} denotes the tangential stress that the liquid of increasing y exerts on a plane surface normal to y-axis and in the x direction. Similarly, p_{zx} is the tangential stress which the

liquid of increasing z exerts on a plane surface normal to z-axis and in the direction of x. Analogous definitions apply to p_{xy} and p_{yz} recalling that the first letter of the subscript refers to the plane acted upon and the second to the direction of the stress. Specializing for the problem at hand, in the absence of wind

$$p_{zx} = 0 \ , \quad z = H = h_w + h_s$$

$$p_{xz} = \tau_s \ , \quad z = h_s \tag{74}$$

where τ_s is the traction of the fresh water on the saline water below. It is a positive quantity and will be referred to as the interfacial stress. Denoting the resistive force of the vertical wall by τ_w, a positive quantity,

$$p_{yx} = -\tau_w \ , \quad y = b$$

$$p_{yx} = \tau_w \ , \quad y = -b \tag{75}$$

47. Equation 73 may be simplified. Multiply the terms of this equation by h_w/U^2, U is the freshwater mean velocity; the result is

$$\frac{u^2}{U^2} h_w \frac{\partial}{\partial x}\left(\frac{w}{u}\right) = -g \frac{h_w}{U^2} + \frac{1}{\rho} \frac{h_w}{U^2} \left(- \frac{\partial p}{\partial z} + \frac{\partial p_{xz}}{\partial x} + \frac{\partial p_{yz}}{\partial y} \right) \tag{76}$$

When the entrainment velocity U_m and the interfacial slope each are small quantities, the expression $h_w \frac{\partial}{\partial x}\left(\frac{w}{u}\right)$ would practically equate the ratio of the freshwater depth to the radius of curvature of the interfacial line. In channels of horizontal bottom, this ratio is a small quantity and hence the left-hand term of the above equation can be neglected. Next, introducing the fluctuations

$$\frac{u'}{U} = \varepsilon_1 \ , \ \frac{v'}{U} = \varepsilon_2 \ , \ \frac{w'}{U} = \varepsilon_3$$

and writing

$$\zeta = \frac{x}{L} \ , \ \eta = \frac{z}{h_w}$$

here L is the total length of the saline water layer, we may place

$$\frac{1}{\rho}\frac{h_w}{U^2}\frac{\partial p_{xz}}{\partial x} = \frac{h_w}{L}\frac{\partial}{\partial \zeta}\overline{\varepsilon_1 \varepsilon_3} \quad \text{and} \quad \frac{1}{\rho}\frac{h_w}{U^2}\frac{\partial p_{yz}}{\partial y} = \frac{\partial}{\partial \zeta}\overline{\varepsilon_2 \varepsilon_3}$$

where ε_1, ε_2, and ε_3 are known to be small quantities. Hence, for the case $gh_w/U^2 > 1$ the last two terms of Equation 76 can also be neglected, leaving

$$0 = -g - \frac{1}{\rho}\frac{\partial p}{\partial z} \tag{77}$$

which indicates that the pressures are hydrostatic. Integrating with respect to z, assuming that the atmospheric pressure is reduced to zero and assuming that entrainment hardly modifies the picture of the densities, this yields

$$p = \rho g(H - z), \quad z > h_s \tag{78}$$

The corresponding relation for the saline water layer is

$$p = \rho g(H - z) + \Delta\rho_s g(h_s - z) \tag{79}$$

where $\Delta\rho_s$ represents the excess of saline water density over that of the fresh water.

48. In the case that mixing across the interface is appreciable, the pressure term for the fresh layer need be expressed in greater detail. For simplicity it will be assumed that the densities in cross sections are averaged and the average value is $\rho + \Delta\rho'$, $z > h_s$, and $\Delta\rho'$ is inferior to $\Delta\rho_s$. One has instead of the form in Equation 78

$$p = (\rho + \Delta\rho')g(H - z), \quad 2 > h_s$$

yielding

$$\frac{1}{\rho}\frac{\partial p}{\partial x} = g\frac{\partial H}{\partial x} + g(H - z)\frac{\partial}{\partial x}\frac{\Delta\rho'}{\rho}$$

Integrating with respect to z between limits h_s and H

$$\int_{h_s}^{H}\frac{1}{\rho}\frac{\partial p}{\partial x}\,dz = g\frac{\partial H}{\partial x}h_w + \frac{g}{2}h_w^2\frac{\partial}{dx}\frac{\Delta\rho'}{\rho}$$

But by continuity of mass, nearly

$$\int_o^x \Delta\rho_s U_{mo}\, dx = U\Delta\rho' h_w \ , \ U_{mo} = \frac{1}{2} U_{m1} + U_{m2}$$

and thus

$$\int_{h_s}^{H} \frac{1}{\rho} \frac{\partial p}{\partial x}\, dz = g \frac{\partial H}{\partial x} h_w + g \frac{h_w}{2} \frac{\Delta\rho_s}{\rho} \frac{U_{mo}}{U} \tag{80}$$

Hence, if mixing is appreciable the term $-g \frac{h_w}{2} \frac{\Delta\rho_s}{\rho} \frac{U_{mo}}{U}$ need be introduced into the right-hand side of Equation 89.

49. Integrating Equation 72 with respect to z, between the limits H and h_s, taking p from Equation 78 and using the relation

$$H = H_o - \delta \ , \tag{81}$$

where H_o is the initial value of H at $x = 0$ and δ is the fall of the water surface, one now has

$$\int_o^H \frac{\partial u^2}{\partial x}\, dz + (uw)_H - (uw)_{h_s} = g \frac{d\delta}{dx} h_w + \frac{1}{\rho}\int_{h_s}^{H} \frac{\partial p_{yx}}{\partial y}\, dz - \frac{\tau_s}{\rho} \tag{82}$$

In the presence of entrainment

$$w_i = w_{h_s} = u_i \frac{\partial h_s}{\partial x} + U_m \tag{83}$$

where u_i and U_m are the interface and entrainment velocities, respectively. Also,

$$w_H = u_s \frac{\partial H}{\partial x} \tag{84}$$

u_s being the velocity at the water free surface. The left-hand member of Equation 82 in view of these now changes to

$$\int_{h_s}^{H} \frac{\partial u^2}{\partial x}\, dz + u_s^2 \frac{\partial H}{\partial x} - u_i^2 \frac{\partial h_s}{\partial x} - u_i U_m \tag{85}$$

Introducing the vertically averaged velocity u at a given y and the Boussinesq coefficient α

$$\alpha \bar{u}^2 h_w = \int_{h_s}^{H} u^2 \, dz \, , \quad h_w = H - h_s \tag{86}$$

Differentiating with respect to x in accordance with Leibnitz rule and assuming α to be independent of x

$$\alpha \frac{\partial}{\partial x}\left(\bar{u}^2 h_w\right) = \int_{h_s}^{H} \frac{\partial u^2}{\partial x} \, dz + u_s^2 \frac{\partial H}{\partial x} - u_i^2 \frac{\partial h_s}{\partial x} \tag{87}$$

Finally, utilizing Equations 85 and 87, Equation 82 changes to

$$\alpha \frac{\partial}{\partial x}\left(\bar{u}^2 h_w\right) - u_i U_m = g \frac{d\delta}{dx} h_w + \frac{1}{\rho}\int_{h_s}^{H} \frac{\partial p_{yx}}{\partial y} \, dz - \frac{\tau_s}{\rho} \tag{88}$$

Next, multiplying the terms in this equation by dy, and integrating between the limits b and $-b$ and then dividing by B, the channel width,

$$\alpha \frac{\partial}{\partial x}\left(U^2 h_w\right) - U_i U_m = g \frac{d\delta}{dx} h_w - \frac{2\tau_w}{\rho} \frac{h_w}{B} - \frac{\bar{\tau}_s}{\rho} \tag{89}$$

when U represents the freshwater mean velocity over a cross section and U_i and U_m are the average values of u_i and u_m across the channel width. It is tacitly assumed that the individual values u_i and u_m differ but little from their average values. This is done for simplicity for otherwise the aim of accuracy would require coefficients difficult to obtain. The total wall shear averaged over the depth h_w is denoted by $\bar{\tau}_w$. In view of the mass flow condition of continuity, Equation 89 may be modified further. Subject to Boussinesq approximation

$$U h_w = q + U_m x \tag{90}$$

where q is the initial water discharge at $x = 0$ computed per unit width of channel. Assuming that U_m is independent of x, it may be shown that

$$\frac{\partial}{\partial x}\left(U^2 h_w\right) = 2U_m U - U^2 \frac{dh_w}{dx}$$

Since the slope of surface water is negligible in comparison with the slope of interface

$$\frac{\partial h_w}{\partial x} = -\frac{\partial h_s}{\partial x}$$

then the last relation may be written as

$$\frac{\partial}{\partial x}\left(U^2 h_w\right) = 2U_m U + U^2 \frac{dh_s}{dx} \tag{91}$$

Introducing this in Equation 89 and afterward dividing the terms of the resulting equation by U^2, one obtains for the freshwater layer the final form of the momentum equation

$$\frac{\bar{\tau}_s}{\rho U^2} = \frac{gh_w}{U^2}\frac{d\delta}{dx} - \frac{\lambda_o h_w}{B} - \alpha\frac{dh_s}{dx} - \left(2\alpha - \frac{U_i}{U}\right)\frac{U_m}{U} \tag{92}$$

with

$$\lambda_o = \frac{2\bar{\tau}_w}{\rho U^2}$$

Needless to state, the last term in Equation 92 shows the effect of entrainment on the momentum equation.

Hydrodynamics of Saltwater Layer

50. During the experiments in order to maintain a constant disposition of the interface, saline waters were introduced laterally at the two ends of the channel. This was meant to balance the entrainment inflow into the flowing fresh water. The same result could have been effected equally well if the inflow was introduced laterally at the level of channel bottom and equally distributed along the entire channel length. The hydrodynamics of the saline layer will be developed for this latter case.

51. Again multiplying the terms in Equation 72 by dz, but now

integrating between the limits $z = 0$ and $z = h_s$ and taking p from Equation 80 and since $U = 0$ at $z = 0$,

$$\int_0^{h_s} \frac{\partial u^2}{\partial x} dz + (uw)h_s = g\left(\frac{d\delta}{dx} - \frac{\Delta\rho_s}{\rho}\frac{dh_s}{dx}\right)h_s + \frac{1}{\rho}\int_0^{h_s} \frac{\partial p_{yx}}{\partial y} dz + \frac{\tau_s}{\rho} + \frac{\tau_o}{\rho} \qquad (93)$$

where τ_o is the bottom stress. This is a positive quantity as the flow adjacent to bottom is in the opposite direction of the freshwater flow. We can write the left-hand member in the form

$$\int_0^{h_s} \frac{\partial u^2}{\partial x} dz + u_i^2 \frac{dh_s}{dx} + u_i u_m \qquad (94)$$

As the average value of u in a cross section vanishes we resort to U_i to form an expression similar to Equation 86. Introducing a new coefficient β

$$\beta U_i^2 h_s = \int_0^{h_s} u^2 dz \quad , z < h_s \qquad (95)$$

Differentiating with respect to x

$$\beta \frac{\partial}{\partial x}\left(U_1^2 h_s\right) = \int_0^{h_s} \frac{\partial u^2}{\partial x^2} dz + u_i^2 \frac{dh_s}{dx} \qquad (96)$$

Utilizing Equations 95 and 96, Equation 93 may be written as

$$\beta \frac{\partial}{\partial x}\left(u_i^2 h_s\right) + M_i U_m = g\left(\frac{d\delta}{dx} - \frac{\Delta\rho_s}{\rho}\frac{dh_s}{dx}\right)h_s + \frac{1}{\rho}\int_0^{h_s} \frac{\partial p_{yx}}{\partial y} dz + \frac{\tau_s}{\rho} + \frac{\tau_o}{\rho} \qquad (97)$$

Multiplying the terms of this equation by dy, integrating between the limits b and $-b$ and dividing the terms of the resulting equation by U^2B

$$\frac{\tau_s}{\rho U^2} + \frac{\tau_o}{\rho U^2} = \frac{gh_s}{U^2}\left(-\frac{d\zeta}{dx} + \frac{\rho_w - \rho_s}{\rho}\frac{dh_s}{dx}\right) + \frac{f_i}{2}\frac{U_1^2}{U^2}\frac{dh_s}{dx} + \lambda_1\frac{h_s}{B} + \frac{U_m U_i}{U^2} \qquad (98)$$

$$\lambda_1 = \frac{2\tau_w}{\rho U^2} \qquad (99)$$

which is the momentum equation relating to the saline layer. Subtracting Equation 92 from Equation 98 there results

$$\frac{\tau_o}{\rho U^2} = -\frac{gH}{U^2}\frac{d\zeta}{dx} + \frac{gh_s}{U^2}\frac{\rho_w - \rho_s}{\rho}\frac{dh_s}{dx} + \frac{f_i}{2}\frac{dh_s}{dx} + \lambda_o\frac{h_w}{B} + \lambda_1\frac{h_s}{B} + 2\varepsilon\frac{U_m}{U} \qquad (100)$$

$$\tau_1 = \left[\alpha + \beta\left(\frac{U_1}{U}\right)^2\right]$$

the expression to evaluate the channel bottom stress.

Experimental Evaluation of Stresses

52. The evaluation of the interfacial stress coefficient will be effected neglecting the entrainment term; that is, using

$$\frac{\tau_s}{\rho U^2} = \frac{gh_w}{U^2}\frac{d\zeta}{dx} - \lambda_o\frac{h_w}{B} - \varepsilon\frac{dh_s}{dx} \qquad (101)$$

In the case of the bottom stress, the entrainment term will be retained but the quantity $\lambda_1 h_s/B$ will be ignored; that is, using

$$\frac{\tau_o}{\rho U^2} = -\frac{gH}{U^2}\frac{d\zeta}{dx} + \frac{gh_s}{U^2}\frac{\rho_w - \rho_s}{\rho}\frac{dh_s}{dx} + \lambda_o\frac{h_w}{B} + \frac{f_i}{2}\frac{dh_s}{dx} + 2\varepsilon\frac{U_m}{U} \qquad (102)$$

It is sufficient to place U_m/U equal to 1.5×10^{-4}. Saline liquid in contact with the vertical walls at the upper and lower parts moves in opposite directions and this fact makes τ_1 a negligible quantity. The observed values of the quantities u, h_w, h_s, dh_s/dx, $d\zeta/dx$ are given in Table 24. On the basis of the data in Tables 6 and 7, λ_o proves to be 1.01 and λ_1, 0.05. Since $U_1/U = 0.54$, $(U_1/U_m)^2$ equals 0.014. In conformity with the law of Blasius, the wall stress due to the flow of fresh water is

$$\frac{\tau_w}{\rho} = a\bar{u}^2 \left(\frac{\bar{u}b}{\nu}\right)^{-1/4} , \quad a = 0.0225 \tag{103}$$

where $\bar{u}$ is the average velocity at z, averaged over the width from $y = -b$ to $y = b$. On this basis

$$\frac{\tau_w}{\rho U^2} = aA \left(\frac{Ub}{\nu}\right)^{-1/4} \tag{104}$$

where

$$A = \int_0^1 \left(\frac{u}{U}\right)^{-8/7} d\eta , \quad \eta = \frac{z}{h_w}$$

Using the data in Table 4, integration yields $A = 0.958$ and that

$$\lambda_o = \frac{2\tau_w}{\rho U^2} = 0.0432 \left(\frac{Ub}{\nu}\right)^{-1/4} \tag{105}$$

Determinations of λ_o for the tests are completed in Table 24. In the same table are shown also $\lambda_o h_w/B$ and dh_s/dx. These quantities are of the same order and as it cannot be guaranteed that the friction of the wall is determined with the same accuracy as the interfacial slope, it would be preferable to conduct tests with wider channels.

53. The computed values of $\bar{\tau}_s$ on the basis of Equation 31 are entered into the third column of Table 25 and these are shown in Figure 37. Pedersen (1980) using the results of various investigations arrived at the following expression for the interfacial stress coefficient. Writing

$$\left.\begin{aligned} f_i/2 &= \tau_i/\rho \ (U_m - U_i)^2 \\ R_i &= (U_m - U_i) \ (y - y_o)/\nu \end{aligned}\right\} \tag{106}$$

the expression is

$$\sqrt{2/f_i} = 2.45 \left[\ln\left(R_i\sqrt{f_i/2}\right) - 1.3\right] \tag{107}$$

This relation is meant to apply equally to saline underflow and freshwater

Table 9

Interface Layer Effective Thickness, l_i

(Observed at x = 2,000 cm)

$\Delta\rho_s/\rho$	Run	U, cm/sec	h_w, cm	l_i, cm	h_w/l_i
0.02	39B	2.58	14.6	0.80	18.2
	40B	39.0	14.3	0.70	20.4
	41B	5.12	14.4	0.74	19.5
	42B	7.31	15.3	0.75	20.4
	43B	9.28	16.0	0.95	16.8
	44B	9.62	19.3	1.06	18.3
	45B	10.95	21.5	1.22	17.6
0.04	9	10.38	17.2	0.84	19.8
	18	5.54	13.4	0.70	19.2
	19	8.06	13.8	0.70	19.7
	20	9.45	15.7	0.67	23.5
	21	10.67	17.4	0.79	22.1
	22	12.95	18.2	0.91	26.0
	23	14.10	20.3	1.13	18.0
0.06	24A	5.36	14.0	0.67	20.8
	25A	7.96	14.2	0.70	20.0
	26A	10.24	16.3	0.70	23.2
	27A	12.30	15.1	0.68	22.2
	28A	14.28	16.5	0.76	21.7
	29A	15.78	18.1	0.76	23.4
	30A	16.70	20.1	0.88	22.6

Table 7

Water-Surface Velocities

$\Delta\rho_s/\rho = 0.06$

Run	24	25	26	27	28	29	30	Mean
U, cm/sec	5.46	8.01	10.25	11.76	13.50	15.09	15.73	
x/L	U_s/U							
0.095	1.144	1.196	1.206	0.949	1.075	0.942	1.030	1.077
0.319	1.137	1.196	1.161	1.066	1.023	1.090	1.127	1.114
0.540	1.067	1.160	1.140	1.121	1.094	1.069	1.102	1.107
0.768	1.133	1.136	1.070	1.059	1.168	1.102	1.078	1.099
0.940	1.050	1.048	1.182	1.160	1.123	1.127	1.111	1.114

Table 8

Interfacial Velocities

$\Delta\rho_s/\rho = 0.06$

Run	24	25	26	27	28	29	30	Mean
U, cm/sec	5.46	8.01	10.25	11.76	13.50	15.09	15.73	
x/L	U_i/U							
0.095	0.493	0.523	0.538	0.578	0.561	0.570	0.535	0.542
0.319	0.552	0.576	0.540	0.566	0.560	0.547	0.535	0.552
0.540	0.495	0.555	0.517	0.515	0.540	0.526	0.511	0.507
0.768	0.427	0.524	0.514	0.520	0.493	0.533	0.483	0.507
0.440	0.492	0.501	0.475	0.516	0.440	0.503	0.464	0.484

Table 6

Velocity Distribution in Saline Water Pool

$\Delta\rho_s/\rho$	0.02	0.04	0.06	Mean
$-z'/h_s$		u/U		
0.00	0.540	0.540	0.540	0.540
0.02	0.390	0.415	0.390	0.347
0.04	0.306	0.286	0.266	0.286
0.06	0.258	0.204	0.191	0.216
0.10	0.197	0.135	0.124	0.152
0.15	0.145	0.079	0.080	0.101
0.20	0.108	0.045	0.055	0.069
0.30	0.064	0.000	0.015	0.026
0.40	0.035	-0.030	-0.014	-0.003
0.50	-0.033	-0.052	-0.055	-0.047
0.60	-0.043	-0.070	-0.061	-0.057
0.70	-0.118	-0.080	-0.100	-0.100
0.80	-0.125	-0.079	-0.095	-0.100
0.85	-0.115	-0.063	-0.070	-0.082
0.90	-0.098	-0.061	-0.068	-0.076
0.95	-0.062	-0.041	-0.040	-0.047
1.00	-0.000	-0.000	-0.000	-0.000

Table 5

Velocity Distribution in Saline Water Pool

$\Delta\rho_s/\rho = 0.040$; $h_s + h_w = 30.3$ cm

Run	18	19	20	21	22	23	Mean
h_s, cm	17.0	16.6	15.3	14.8	12.2	10.3	
U, cm/sec	5.54	8.06	9.45	10.61	12.95	14.10	
$-z'/h_s$	u/U						
0.00	0.540	0.540	0.540	0.540	0.540	0.540	0.540
0.02	0.470	0.440	0.340	0.420	0.400	0.420	0.415
0.04	0.390	0.200	0.210	0.270	0.280	0.370	0.286
0.06	0.310	0.120	0.140	0.160	0.180	0.320	0.204
0.10	0.200	0.070	0.070	0.100	0.135	0.235	0.135
0.15	0.120	0.035	0.020	0.050	0.080	0.170	0.079
0.20	0.080	0.020	-0.010	0.010	0.040	0.130	0.045
0.30	0.000	-0.010	-0.035	0.020	-0.010	0.070	0.000
0.40	-0.045	-0.025	-0.040	-0.020	-0.050	0.000	-0.030
0.50	-0.075	-0.040	-0.040	-0.020	-0.080	-0.060	-0.052
0.60	-0.095	-0.050	-0.040	-0.020	-0.100	-0.110	-0.070
0.70	-0.105	-0.055	-0.040	-0.020	-0.120	-0.140	-0.080
0.80	-0.110	-0.055	-0.040	-0.020	-0.110	-0.140	-0.079
0.85	-0.100	-0.050	-0.040	-0.020	-0.100	-0.130	-0.063
0.90	-0.090	-0.040	-0.035	-0.020	-0.080	-0.100	-0.061
0.95	-0.060	-0.035	-0.020	-0.010	-0.050	-0.070	-0.041
1.00	-0.000	-0.000	-0.000	-0.000	-0.000	-0.000	-0.000

Table 4

Velocity Distribution in Freshwater Current

$\Delta\rho_s/\rho$	0.02	0.04	0.06	Mean
z'/h_w		u/U		
0.00	0.540	0.540	0.540	0.540
0.02	0.668	0.680	0.676	0.675
0.04	0.775	0.771	0.786	0.777
0.06	0.853	0.845	0.865	0.854
0.08	0.908	0.882	0.906	9.898
0.10	0.948	0.911	0.937	0.932
0.12	0.971	0.935	0.960	0.955
0.16	1.012	0.965	0.995	0.991
0.20	1.035	0.989	1.015	1.013
0.30	1.055	1.020	1.040	1.037
0.40	1.061	1.035	1.052	1.049
0.50	1.061	1.042	1.052	1.049
0.60	1.052	1.042	1.048	1.047
0.70	1.032	1.032	1.032	1.032
0.80	1.003	1.028	1.015	1.015
0.90	0.970	1.010	0.995	0.992
1.00	0.935	0.991	0.968	0.965

Table 3

Velocity Distribution in Freshwater Current

$\Delta\rho_s/\rho = 0.040$; $h_s + h_w = 30.3$ cm

Run	18	19	20	21	22	23	Mean
h_w, cm	13.3	16.6	15.3	14.8	12.2	10.3	
U, cm/sec	5.54	8.06	9.45	10.61	12.95	14.10	
z'/h_w	u/U						
0.00	0.54	0.54	0.54	0.54	0.54	0.54	0.540
0.02	0.68	0.67	0.70	0.72	0.66	0.65	0.680
0.04	0.80	0.79	0.79	0.81	0.75	0.73	0.771
0.06	0.88	0.86	0.85	0.85	0.81	0.81	0.845
0.08	0.92	0.91	0.89	0.89	0.84	0.84	0.882
0.10	0.95	0.94	0.92	0.91	0.88	0.86	0.911
0.12	0.97	0.95	0.94	0.93	0.91	0.90	0.935
0.16	1.00	0.98	0.98	0.96	0.95	0.92	0.965
0.20	1.02	0.99	1.00	0.98	0.98	0.96	0.989
0.30	1.04	1.02	1.04	1.01	1.01	1.01	1.020
0.40	1.04	1.03	1.05	1.03	1.03	1.03	1.035
0.50	1.04	1.04	1.06	1.04	1.04	1.04	1.042
0.60	1.03	1.04	1.06	1.05	1.04	1.05	1.042
0.70	1.01	1.03	1.05	1.04	1.04	1.05	1.032
0.80	1.00	1.02	1.04	1.03	1.04	1.05	1.028
0.90	0.97	1.00	1.02	1.01	1.02	1.04	1.010
1.00	0.95	0.98	1.00	0.99	1.00	1.03	0.991

Table 2

Dependence of Rise of Interface and Fall of Water Surface on Densimetric Froude Number

Run	$\Delta\rho$	$10^6\ d\delta/dx$	$10^4U^2/gH_w$	$10^4U^2/gH_o$	$10^4dh_s/dx$	$10^2 \times U^2/\frac{\Delta\rho}{\rho}\ gh_w$
34	0.02	3.75	4.69	2.21	2.92	2.34
40		7.36	13.60	5.96	5.6	7.80
41		10.95	18.50	8.76	8.3	9.25
42		20.91	33.10	16.98	14.5	11.55
43		30.00	41.80	24.08	21.5	20.70
44		33.40	43.40	28.6	26.0	21.70
45		42.40	48.80	36.2	25.0	24.40
10	0.04	24.2	34.6	17.4	10.0	8.72
11		29.3	47.0	26.0	15.0	11.7
12		33.8	47.0	26.0	15.0	11.7
13		47.1	61.8	36.3	18.0	15.8
14		55.4	67.8	45.1	24.5	16.9
16		72.6	83.1	58.8	30.5	20.8
17		13.7	20.5	9.38	8.0	5.12
24	0.06	11.8	21.9	9.80	4.5	3.84
25		23.4	47.1	21.6	6.6	7.85
26		43.1	73.4	34.9	10.0	12.28
27		55.4	94.4	47.7	13.4	15.70
28		72.0	107.2	61.2	17.8	17.80
29		82.4	110.5	71.4	21.8	18.40
30		92.2	117.0	82.1	26.0	19.50

Table 1

Rates of Rise of Interface and Fall of Water Surface

$H_o = h_s + h_w + \delta$; H_1 - 30.3 cm

Run	$\Delta\rho/\rho$	g, cm^2/sec	h_s, cm	$dh_s/dx^4 \times 10^4$	$d\delta/dx \times 10^6$
39	0.020	37.1	17.8	2.9	3.75
40		55.7	16.9	5.6	7.36
41		74.2	15.8	8.3	10.45
42		111.3	14.7	14.5	20.91
43		148.4	12.8	21.5	30.00
44		185.6	10.2	26.0	33.40
45		235.7	7.7	25.0	42.40
10	0.040	111.3	14.9	10.0	24.2
11		148.4	13.5	15.0	29.3
12		148.4	13.5	15.0	33.8
13		185.6	12.5	18.0	47.1
14		235.7	10.0	24.5	55.4
16		285.7	8.8	30.8	72.6
17		74.2	16.3	8.0	13.7
24	0.060	74.2	16.6	4.5	11.8
25		111.3	16.4	6.6	23.4
26		148.4	15.8	10.0	43.1
27		185.6	14.8	13.4	55.4
28		235.7	12.9	17.8	72.0
29		285.8	10.7	21.8	82.4
30		335.8	8.9	22.0	92.2

Note: h_s measured at station x = 2,000 .

REFERENCES

Anwar, H. O., and Weller, J. A., 1981. "An Experimental Study of the Structure of Freshwater-Saltwater Interfacial Mixing," La Houille Blanche, Vol 6.

Ellison, T. H., and Turner, J. S., 1959. "Turbulent Entrainment in Stratified Flows," Journal of Fluid Mechanics, Vol 6, Part 3.

Huppert, H. E., and Britten, R. E., 1982 (Dec). "Separation of Hydraulic Flow over Topography," Journal Hydraulics Division, American Society of Civil Engineers, Vol 108, No. HY12.

Keulegan, G. H., 1949 (Oct). "Fourth Progress Report on Model Laws of Density Currents," Report to Chief of Engineers, US Army, Washington, DC.

_____. 1955 (Jul). "Seventh Progress Report on Model Laws of Density Currents; Interface Mixing in Arrested Saline Wedges," NBS Report No. 4142, Report to Director, US Army Engineer Waterways Experiment Station, Vicksburg, Miss.

Loftquist, Karl 1960 (Apr). "Flow and Stress near an Interface Between Stratified Liquids," The Physics of Fluids, Vol 3, No. 2.

Pedersen, F. B. 1980. "A Monograph on Turbulent Entrainment and Friction of Two Layer Stratified Flow," Institute of Hydrodynamics and Hydraulic Engineering, Technical University of Denmark, Lyngby.

Suga, Kyozo 1975 (Jul). "Salt Wedge Intrusion with Entrainment." International Association for Hydraulic Research, Sao Paulo, Brazil.

The purpose of these requirements is to see if the conditions at the ends have any bearing on the mixing across the interface. A channel of 30-m length and of 40-cm height suffices. To minimize the uncertainties relating to the vertical wall stresses, it is desirable that the channel be wide, say, at least 90 cm. The liquid height in channel may be chosen as 30 cm, with an underlying saline layer depth of 15 or 20 cm. The saline water may be introduced from a special tank, the inflow into channel being either from the bottom vertically upward or from the channel wall laterally at the level of the bottom, the flow distribution being uniform in both cases along the entire length of the bottom. Care is taken to measure accurately the quantity of saline inflow to assure a correct balance with the transport of saline water across the interface. The densities may be measured by parallel wire electrodes in one of the following manners. The liquids from different levels may be sucked and collected in separate bottles in the manner effected by Loftquist (1960). The densities of the collected samples in bottles can be measured in later times. Or the electrode may be attached to a gage which may be moved vertically through the entire depth for the local measurement of densities. In the latter case, it is desirable to calibrate the electrode in moving saline water. This is a matter of a long investigation. The liquid velocities may be measured by deflecting ribbons as in the present tests. To avoid errors of uncertain zero readings, the deflections may be determined through strain gage indications, the gages being attached to the ribbon at its clamped area. To show that the method is feasible also a separate investigation would be required. The fall of water surface may be measured by five optical manometers of the type used in the present study. For accuracy, however, it is necessary that each manometer is provided with individual telescopes. Then, the front cells of the manometer are connected to a tank or a trough channel of constant surface level attached to an experimental channel and the hinder cells to the channel at five distant points with equal spacing between them.

In this study then as Figure 38 shows, the flow adjacent to the bottom is laminar and the stress would be

$$\tau_o = 2\mu \frac{u_m}{d_m} \tag{117}$$

or in terms of h_s and U

$$\frac{\tau_o}{\rho U^2} = \frac{2u_m}{U} \frac{h_s}{d_m} \left(\frac{Uh_s}{\nu}\right)^{-1} \tag{118}$$

Using the values of u_m/U and h_s/d_m mentioned above

$$\frac{\tau_o}{\rho U^2} = 1.5 \left(\frac{Uh_s}{\nu}\right)^{-1}$$

Comparing with Equation 112 it is seen that the estimate of the stress from the observed velocities is ten times smaller than that computed from the hydrodynamic Equation 101.

56. The severe disagreement between the two determinations of the bottom stress above indicated is disappointing. The cause of the disagreement in one part is the difficulty of low flow measurements and in another part, the inaccuracies in the measurements of layer depths and slopes of interface and of upper free surface. Also the method of evaluating the vertical wall stresses is open to question. Further, probably Equation 102 does not take into account the actual saline flow conditions met with in the tests. It will be remembered that to balance the saline water transfer across the interface, saline flows were introduced laterally at the channel's two extreme ends. The dynamic effect of these flows on the saline layer was not considered in developing Equation 102.

Recommendations for a New Research

57. In view of the fact that the dependence of the transport of saline water across the interface upon densimetric Froude number is not in agreement with the results of other investigations, it is desirable that the problem be considered in a modified channel specially in order to pay attention to a possible mixing in the area of the freshwater entrance. In the new channel, the bottom is inclined at the entrance and the efflux is over a weir.

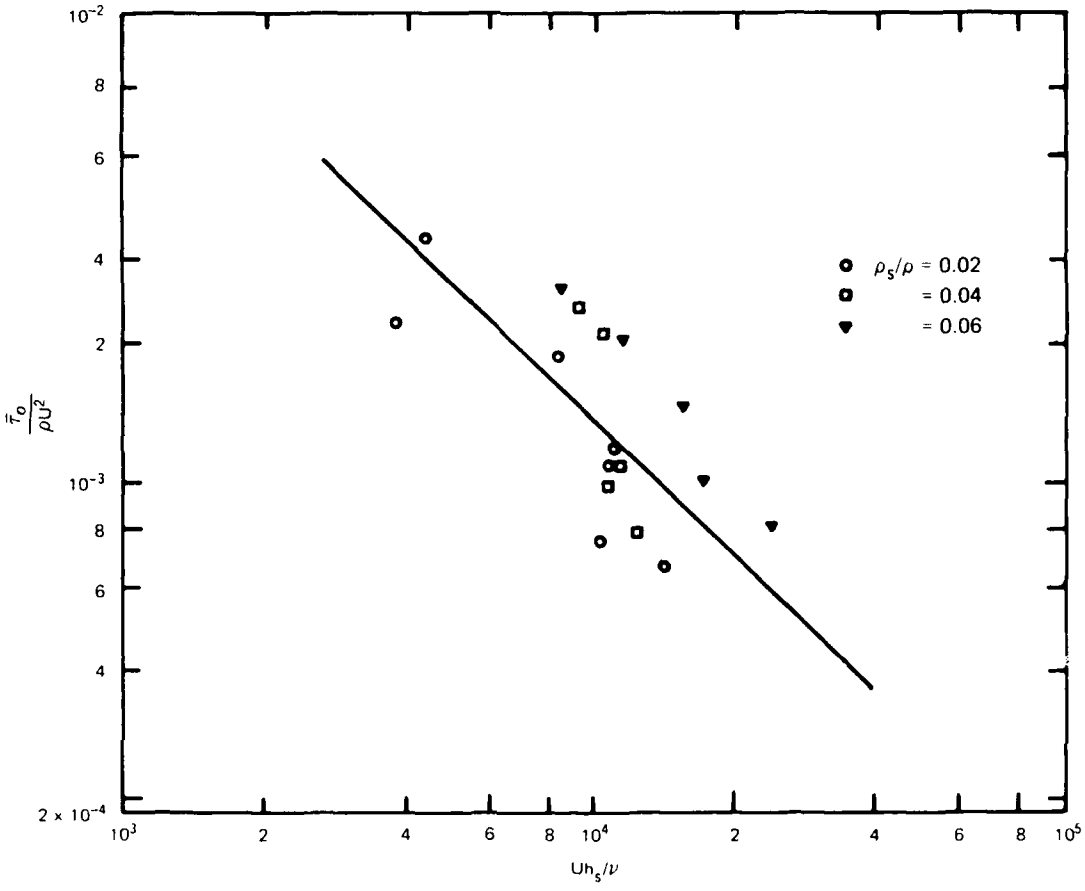

Figure 38. Dependence of bottom stress on Reynolds number

$$\bar{u} = \frac{2}{3} u_m \tag{114}$$

In terms of U and h_s the criterion may now be written also as

$$\frac{Uh_s}{\nu} < 900 \frac{h_s}{d_m} \frac{U}{u_m} \tag{115}$$

From Figure 15, representing the velocities of the salt layer, one may take $u_m/U = 0.15$ and $d_m/h_s = 0.2$. Using these values, the condition for the luminary regime in the part adjacent to the bottom is

$$\frac{Uh_s}{\nu} < 41,500 \tag{116}$$

$$\frac{\bar{\tau}_s}{\rho U^2} = 0.066 \left(\frac{U h_w}{\nu} \right)^{-1/3} \tag{110}$$

which is equally useful as the logarithmic form and is based on scattered data.

54. For the evaluation of the interfacial stress when the fall of the water surface is not obtainable, one may proceed supposing that the momentum effects in the saline water are negligible. Pedersen proceeded on this basis to obtain data from various authors to establish the relation presented by Equation 107. To proceed in the same manner for the present investigation, one obtains by eliminating $d\delta/dx$ from Equations 92 and 98 after ignoring the momentum effects in the second equation, the result

$$\frac{\bar{\tau}_s}{\rho U^2} = \frac{\left(\frac{g h_w}{U^2} \frac{\Delta\rho_s}{\rho} - 1 \right) \frac{dh_s}{dx} - \lambda_o \frac{h_w}{B}}{1 + h_w \, \iota_s} \tag{111}$$

Evaluations made on this basis are shown in the fourth column of Table 25. The average interfacial shear stress thus evaluated is nearly 30 percent higher than when the bottom stress and momentum effects are not ignored.

55. In Figure 38 the data of the bottom stress, which are given in the fifth column of Table 25, are plotted against the Reynolds number $U h_s/\nu$. Although the scatter of the data points is severe, nevertheless the average distribution may be represented by the straight line drawn with the equation

$$\frac{\tau_o}{\rho U^2} = 15 \left(\frac{U h_s}{\nu} \right)^{-1} \tag{112}$$

The relevance of this result with the measured velocities in the vicinity of the bottom may be next examined. Relying on a result from open channel flow, the criterion for the laminar regime in the layer adjacent is

$$\frac{\bar{u} \, d_m}{\nu} < 500 \tag{113}$$

where $\bar{u}$ is the average velocity in the layer, and d_m the distance of the maximum u_m from the bottom. For a laminar layer

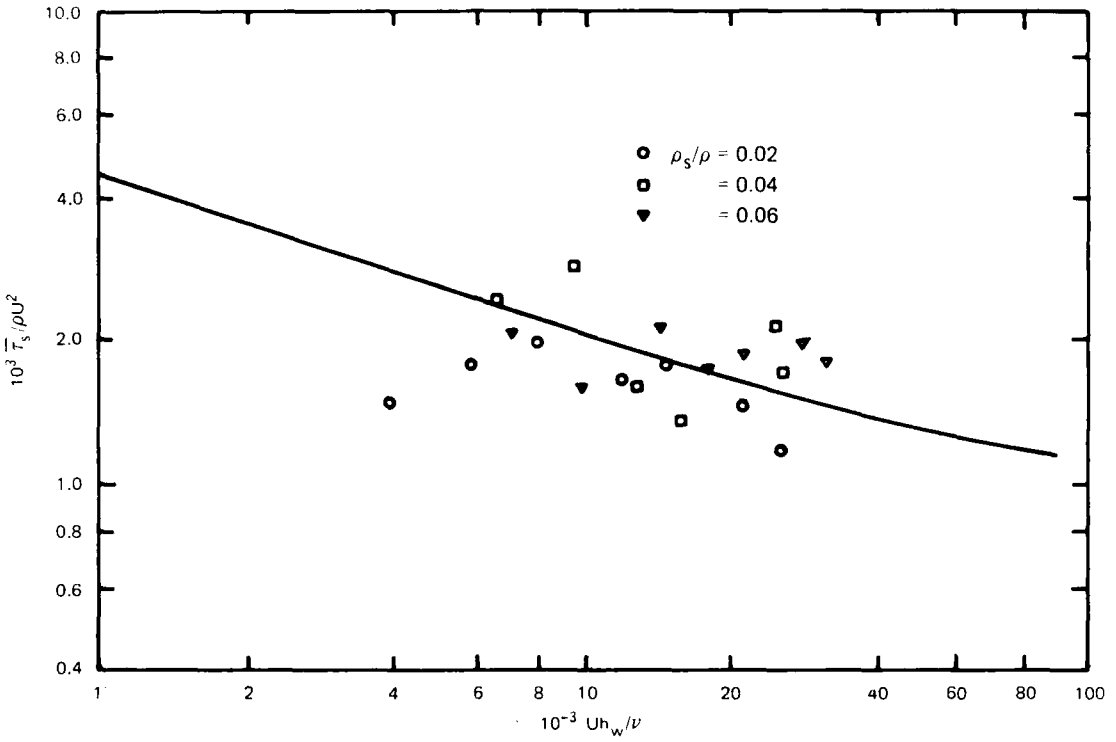

Figure 37. Dependence of interfacial stress on Reynolds number

overflow. Aiming to obtain a relation applying solely to an overflow, we place $U = 1.79\ (U_m - U_i)$ and identify $y - y_o$ with the freshwater depth h_w and next writing

$$\lambda_i/2 = \overline{\tau}_s/\rho U^2 \tag{108}$$

$$R = Uh_w/\nu$$

the Pedersen relation becomes

$$\sqrt{2/\lambda_i} = 3.45\left[\ln\left(R\sqrt{\lambda_i/2}\right) - 1.3\right] \tag{109}$$

The curve shown in Figure 37 is from this relation, and the data points of the present investigation are in fair agreement with the Pedersen formulation. The equivalent formula in a power form is

Table 10

Interface Layer Effective Thickness, l_i

(Observed at x = 3,000 cm)

$\Delta\rho_s/\rho$	Run	U, cm/sec	h_w, cm	l_i, cm	h_w/l_i
0.02	39A	2.64	14.1	0.95	14.8
	40A	4.00	13.9	0.90	15.5
	41A	5.60	13.3	0.85	15.6
	42A	8.12	13.8	1.00	13.8
	43A	10.58	14.0	1.40	10.0
	44A	11.72	15.8	0.90	17.5
	45A	13.60	17.3	1.40	12.2
0.04	1	2.97	12.5	1.15	10.8
	2	3.42	11.3	1.30	8.8
	3	6.58	11.3	0.91	12.4
	4	7.15	15.6	1.08	12.5
	5	10.30	14.4	1.10	13.1
	6	12.70	14.6	1.16	12.6
	7	15.40	15.3	1.50	10.1
	8	17.85	16.1	0.82	19.7
0.06	24	5.85	12.9	0.75	17.2
	25	8.65	12.9	0.65	19.9
	26	11.70	12.7	0.70	18.1
	27	14.30	13.0	0.80	16.4
	28	16.52	14.3	0.90	15.9
	29	17.70	16.0	1.10	14.4
	30	19.80	17.0	1.35	12.5

Table 11

Interface Layer Effective Thickness, l_u

(Observed at x = 2,000 cm)

$\Delta\rho_s/\rho$	Run	U, cm/sec	h_w, cm	l_u, cm	h_w/l_u
0.02	39B	2.58	14.6	2.0	7.30
	40B	3.90	14.3	2.3	6.18
	41B	5.12	14.4	2.1	7.42
	42B	7.31	15.3	2.9	5.80
	43B	9.28	16.0	3.1	5.10
	44B	9.42	19.3	3.3	5.80
	45B	10.95	21.5	3.6	6.02
0.04	9	10.38	17.2	2.2	7.70
	18	5.54	13.4	2.0	6.70
	19	8.06	13.8	1.9	7.18
	20	9.45	15.7	2.5	6.28
	21	10.67	17.4	2.4	7.30
	22	12.95	18.2	2.8	6.58
	23	14.10	20.3	3.6	5.72
0.06	24A	5.36	14.0	1.8	7.84
	25A	7.96	14.0	2.2	6.30
	26A	10.24	16.3	2.5	6.54
	27A	12.30	15.1	2.5	6.02
	28A	14.28	16.5	3.1	5.26
	29A	15.78	18.1	3.0	6.00
	30A	16.70	20.1	3.5	5.60

Table 12

Density and Salinity Relations for Saltwater Solutions

ρ = Density of Water; $\rho + \Delta\rho$ = Density of Saline Solution

$\rho/\rho_m = 0.465$

$\Delta\rho/\rho$	α	S	ε	$S/(\Delta\rho/\rho$
0.0053	1.89	0.01	1.032	1.89
0.0125	1.62	0.02	0.826	1.60
0.0268	1.54	0.04	0.756	1.49
0.0413	1.51	0.06	0.734	1.45
0.0559	1.51	0.08	0.734	1.43
0.0707	1.52	0.10	0.734	1.41
0.0857	1.52	0.12	0.744	1.40
0.1009	1.52	0.14	0.748	1.40

Table 13

Saline Density Distribution in Fresh Water

Run 27B, $\Delta\rho_s/\Delta\rho = 0.06$; $q = 185.6$ cm^2/sec

x = 1,000 cm; U = 11.4 cm/sec

z, ft	$\Delta\rho/\Delta\rho_s$	z, ft	$\Delta\rho/\Delta\rho_s$
-0.095	0.970	0.010	0.159
-0.055	0.970	0.014	0.00734
-0.035	0.970	0.015	0.00648
-0.025	0.941	0.019	0.00546
-0.016	0.922	0.0024	0.00444
-0.006	0.836	0.034	0.00375
-0.005	0.789	0.044	0.00341
-0.001	0.624	0.064	0.00239
0.000	0.508	0.104	0.00188
0.004	0.193	0.204	0.00102
0.005	0.162	0.304	0.00086

Table 14

Saline Density Distribution in Fresh Water

Run 27B, $\Delta\rho/\Delta\rho_s = 0.06$; $q = 185.6$ cm^2/sec

x = 3,000 cm; U = 14.3 cm/sec

z, cm	$\Delta\rho/\Delta\rho_s$	z, cm	$\Delta\rho/\Delta\rho_s$
-0.088	0.895	0.037	0.0123
-0.048	0.886	0.052	0.0097
-0.028	0.861	0.062	0.00846
-0.018	0.844	0.072	0.00665
-0.007	0.768	0.092	0.00511
-0.003	0.613	0.112	0.0046
0.002	0.448	0.162	0.00358
0.007	0.261	0.212	0.00239
0.012	0.0524	0.262	0.00175
0.017	0.0283	0.312	0.00136
0.022	0.0165	0.412	0.00136
0.030	0.0146		

Table 15

Saline Density Distribution in Fresh Water

Run 27B, $\Delta\rho_s/\Delta\rho = 0.06$; $q = 185.6$ cm^2/sec

$x = 2{,}000$ cm; $U = 13.0$ cm/sec

z, ft	$\Delta\rho/\Delta\rho_s$	z, ft	$\Delta\rho/\Delta\rho_s$
-0.043	0.959	0.027	0.0104
-0.033	0.951	0.032	0.00906
-0.023	0.933	0.037	0.00808
-0.013	0.878	0.047	0.00586
-0.008	0.848	0.057	0.00515
-0.003	0.675	0.077	0.00319
0.002	0.364	0.097	0.00279
0.007	0.1039	0.147	0.00195
0.012	0.0320	0.243	0.00142
0.015	0.0156	0.347	0.00080
0.022	0.0114		

Table 16

Saline Transport Across Interface

Run 44C, $\Delta\rho_s/\rho = 0.02$; Run 9, $\Delta\rho_s/\rho = 0.04$; Run 27B, $\Delta\rho_s/\rho = 0.06$

$q \approx 185.6$ cm^2/sec

$\Delta\rho_s/\rho$	10^3L, cm	U, cm/sec	h_w, cm	$2Q_{S2}$, cm^2/sec
0.02	1	7.8	21.3	0.66
	2	8.7	19.0	1.06
	3	9.5	15.3	2.36
0.04	1	7.8	19.3	0.59
	2	8.5	17.4	1.13
	3	9.8	14.5	2.15
0.06	1	10.6	16.2	0.36
	2	11.4	14.2	0.79
	3	12.0	13.2	1.59

Table 17a

$\Delta\rho_s/\rho = 0.02$; L = 2,000 cm; $\nu = 0.0091$

$U = q/h_w$

Run	h_w, cm	U, cm/sec	$10^4 U_{m1}$	$10^4 U_{m2}$
39B	15.8	2.35	3.36	0.06
40B	15.7	3.36	4.52	0.18
41B	15.5	4.78	5.72	0.25
42B	16.3	6.86	9.40	1.00
43B	17.5	8.52	13.62	1.90
44B	20.6	9.05	13.70	2.48
44C	20.7	9.04	12.60	2.90
45B	22.4	10.50	18.90	4.66

Table 17b

$\Delta\rho_s/\rho = 0.02$; L = 3,000 cm; $\nu = 0.0091$

$U = q/h_w$

Run	h_w, cm	U, cm/sec	$10^4 U_{m1}$	$10^4 U_{m2}$
39A	14.6	2.54	3.31	0.03
40A	14.5	3.84	6.00	0.13
41A	14.6	5.05	7.10	0.48
42A	16.0	7.05	10.4	1.48
43A	17.8	8.35	19.0	2.58
44A	20.6	9.00	19.8	3.60
44C	20.6	9.00	16.2	3.63
45A	23.0	10.00	21.4	3.50

Table 18a

$\Delta\rho_s/\rho = 0.04$; L = 2,000 cm; $\nu = 0.0108$

$U = q/h_w$

Run	h_w, cm	U, cm/sec	$10^4 U_{m1}$, cm/sec	$10^4 U_{m2}$, cm/sec
18	14.5	5.08	7.90	0.09
19	14.9	7.40	12.60	0.05
20	16.4	8.68	15.60	0.98
21	19.2	9.70	13.80	2.83
22	19.7	11.90	15.30	4.53
23	22.0	12.95	22.80	8.60

Table 18b

$\Delta\rho_s/\rho = 0.04$; L = 3,000 cm; $\nu = 0.0106$

$U = q/h_w$

Run	h_w, cm	U, cm/sec	$10^4 U_{m1}$, cm/sec	$10^4 U_{m2}$, cm/sec
1	14.2	1.88	3.19	0.01
2	13.6	3.06	5.60	0.08
3	13.9	4.16	7.60	0.28
4	17.8	6.26	10.80	0.29
5	17.8	8.36	14.70	1.68
6	18.0	10.32	16.50	3.70
7	19.6	12.95	25.40	5.80
8	20.3	14.15	27.80	8.18

Table 19a

$\Delta\rho_s/\rho = 0.06$; L = 2,000 cm; $\nu = 0.0098$

$q = Uh_w$

Run	h_w, cm	U, cm/sec	$10^4 U_{m1}$, cm/sec	$10^4 U_{m2}$, cm/sec
24A	15.2	4.85	7.41	0.006
25A	15.2	7.30	10.00	0.017
26A	15.5	9.40	13.52	0.079
27A	16.4	11.30	19.80	2.39
28A	17.8	13.10	19.00	3.45
29A	19.7	14.50	23.10	5.16
30A	21.8	15.35	30.40	7.90

Table 19b

$\Delta\rho_s/\rho = 0.06$; L = 3,000 cm; $\nu = 0.0103$

$q = Uh_w$

Run	h_w, cm	U, cm/sec	$10^4 U_{m1}$, cm/sec	$10^4 U_{m2}$, cm/sec
24	14.15	5.06	7.9	0.088
25	14.4	7.62	11.4	0.37
26	14.8	9.78	15.5	1.75
27	15.9	11.75	19.6	3.85
28	17.8	13.65	21.4	5.12
29	19.5	15.10	23.30	7.10
30	21.0	15.95	29.80	10.10

Table 20a

$\Delta\rho_s/\rho = 0.02$; L = 2,000 cm; $\nu = 0.0091$

Run	$10^4 \frac{U_{m1}}{U}$	$10^4 \frac{U_{m2}}{U}$	$10^4 \frac{U}{Um}$	$10^2 F_\Delta^2$	$10^3 R$
39B	1.42	0.02	1.44	1.77	4.07
40B	1.35	0.05	1.40	3.69	6.10
41B	1.12	0.05	1.17	7.40	8.10
42B	1.37	0.14	1.51	14.82	12.20
43B	1.60	0.22	1.82	21.16	16.28
44B	1.44	0.27	1.71	20.25	20.30
44C	1.39	0.32	1.71	20.25	20.30
45B	1.81	0.44	2.25	25.10	25.80

Table 20b

$\Delta\rho_s/\rho = 0.02$; L = 3,000 cm; $\nu = 0.0091$

Run	$10^4 \frac{U_{m1}}{U}$	$10^4 \frac{U_{m2}}{U}$	$10^4 \frac{U}{Um}$	$10^2 F_\Delta^2$	$10^3 R$
39A	1.33	0.01	1.34	2.02	4.07
40A	1.65	0.03	1.68	4.84	6.14
41A	1.37	0.09	1.46	8.53	8.04
42A	1.35	0.21	1.56	15.8	12.30
43A	1.81	0.31	2.12	19.9	16.20
44A	1.66	0.40	2.06	19.8	20.80
44C	1.73	0.40	2.13	19.8	20.80
45A	1.61	0.35	1.96	24.1	26.00

Table 21a

$\Delta\rho_s/\rho = 0.04$; L - 2,000 cm; $\nu = 0.0108$

Run	$10^4 \frac{U_{m1}}{U}$	$10^4 \frac{U_{m2}}{U}$	$10^4 \frac{Um}{U}$	$10^2 F_\Delta^2$	$10^3 R$
18	1.56	0.02	1.58	4.54	6.08
19	1.70	0.01	1.71	9.36	10.32
20	1.80	0.11	1.91	11.7	13.75
21	13.8	0.29	1.67	12.4	17.22
22	1.28	0.38	1.66	18.2	17.22
23	1.76	0.43	2.19	19.3	21.80

Table 21b

$\Delta\rho_s/\rho = 0.04$; L = 3,000 cm; $\nu = 0.0106$

Run	$10^4 \frac{U_{m1}}{U}$	$10^4 \frac{U_{m2}}{U}$	$10^4 \frac{Um}{U}$	$10^2 F_\Delta^2$	$10^3 R$
1	1.69	0.01	1.70	0.64	3.50
2	1.82	0.03	1.85	1.99	5.28
3	1.82	0.06	1.88	3.13	7.02
4	1.71	0.05	1.76	5.66	10.53
5	1.75	0.21	1.96	9.98	14.02
6	1.59	0.36	1.95	15.2	17.57
7	1.95	0.44	2.35	18.9	22.30
8	1.95	0.58	2.53	25.0	27.10

Table 22a

$\Delta\rho_s/\rho = 0.06$; L = 2,000 cm; $\nu = 0.0098$

Run	$10^4 \frac{U_{m1}}{U}$	$10^4 \frac{U_{m2}}{U}$	$10^4 \frac{Um}{U}$	$10^2 F_\Delta^2$	$10^3 R$
24A	1.53	0.00	1.53	2.66	7.56
25A	1.36	0.00	1.36	6.15	11.34
26A	1.44	0.01	1.45	9.67	15.10
27A	1.95	0.21	1.96	14.7	18.92
28A	1.45	0.26	1.71	16.5	24.00
29A	1.59	0.37	1.96	18.1	29.10
30A	1.98	0.62	2.50	18.4	34.28

Table 22b

$\Delta\rho_s/\rho = 0.06$; L = 3,000 cm; $\nu = 0.0103$

Run	$10^4 \frac{U_{m1}}{U}$	$10^4 \frac{U_{m2}}{U}$	$10^4 \frac{Um}{U}$	$10^2 F_\Delta^2$	$10^3 R$
24	1.55	0.02	1.57	2.99	7.30
25	1.50	0.05	1.55	6.86	10.95
26	1.60	0.18	1.78	10.24	14.10
27	1.67	0.33	2.01	14.1	18.25
28	1.56	0.38	1.94	17.6	23.20
29	1.59	0.52	2.11	19.9	28.00
30	1.87	0.63	2.50	19.8	33.00

Table 23

Measured Quantities Relating to the Stresses

$h_w = H - h_s$; $H = 30.3$ cm; h_s Measured at $x = 2{,}000$ cm

Run	δ_s/δ	h_s, cm	h_w, cm	U, cm/sec	dh_s/dx	$d\bar{\delta}/dx$
39	0.02	17.8	12.5	2.97	2.90×10^{-4}	3.75×10^{-6}
40		16.9	13.4	4.22	5.60	7.36
41		15.8	14.5	5.12	8.30	10.9
42		14.7	15.6	7.12	14.5	20.9
43		12.8	17.5	8.48	21.5	30.0
44		10.2	20.1	9.29	26.0	33.4
45		7.7	22.6	10.42	35.0	42.4
10	0.04	14.9	15.4	7.22	10.0×10^{-4}	24.2×10^{-6}
11		13.5	16.8	8.90	15.0	29.2
12		13.5	16.8	8.80	15.0	35.6
13		12.5	17.8	10.42	18.0	47.1
14		10.0	20.3	11.60	24.5	55.4
16		8.8	21.5	13.26	3.05	72.6
17		16.3	14.0	5.30	8.0	13.7
24	0.06	16.6	13.7	5.42	4.5×10^{-4}	11.8×10^{-6}
25		16.4	13.9	8.00	6.6	23.4
26		15.8	14.5	10.23	10.0	43.1
27		14.8	15.5	11.95	13.4	55.4
28		12.9	17.4	13.55	17.8	72.0
29		10.7	19.6	14.58	21.8	82.4
30		8.9	21.4	15.67	21.0	92.2

Table 24

Coefficient of Resistance of the Channel Sidewalls

2b = 22.7 cm

(U and ν in cgs units)

Run	$\Delta\rho_s/\rho$	$10^3\nu$	$U^{1/4}$	$10^3\lambda_o$	$10^3\lambda_o h_w/B$	$10^3\, dh_s/dx$
39	0.020	9.39	1.31	5.55	3.40	0.29
40			1.43	5.10	3.16	0.56
41			1.50	4.86	3.10	0.83
42			1.54	4.73	3.35	1.45
43			1.71	4.27	3.29	2.25
44			1.73	4.20	3.70	2.60
45			1.79	4.08	4.08	3.50
10	0.040	11.11	1.64	4.64	3.09	1.00
11			1.72	4.41	3.18	1.50
12			1.72	4.41	3.18	1.50
13			1.79	4.25	3.50	1.80
14			1.85	4.11	3.63	2.45
16			1.91	3.98	3.88	3.05
17			1.51	6.00	3.60	0.80
24	0.060	10.07	1.53	4.89	2.98	0.45
25			1.68	4.46	2.72	0.66
26			1.79	4.19	2.70	1.00
27			1.86	4.03	2.78	1.34
28			1.91	3.93	3.06	1.78
29			1.95	3.84	3.29	2.18
30			1.99	3.76	3.50	2.60

Table 25

Experimental Evaluation of Interfacial and Bottom Stresses

$$F_{\Delta} = U/\sqrt{(\Delta\rho_s/\rho)gh_s}$$

Run	$\Delta\rho_s/\rho$	$\bar{\tau}_s/\rho U^2$	$\bar{\tau}_s/\rho U^2$	$\bar{\tau}_o/\rho U^2$	Uh_w/ν	$10F_{\Delta}$
39	0.02	1.48×10^{-3}	2.29×10^{-3}	3.32×10^{-3}	3.93×10^{3}	1.53
40		1.70	2.00	2.20	5.90	2.79
41		1.99	2.61	1.90	7.90	3.03
42		1.64	1.92	1.11	11.92	3.40
43		1.74	2.12	1.19	14.95	4.55
44		1.4	1.92	0.75	19.85	4.66
45		1.16	2.30	0.67	25.10	4.94
10	0.04	2.99×10^{-3}	3.86×10^{-3}	2.80×10^{-3}	9.78×10^{3}	2.45
11		1.54	3.56	2.42	13.02	3.42
12		2.50	3.56	2.42	13.02	3.42
13		1.34	1.81	1.19	15.25	3.98
14		2.10	2.77	0.80	25.10	4.11
16		1.79	2.25	1.09	25.90	4.56
17		2.48	6.42		6.64	2.26
24	0.05	2.08×10^{-3}	4.98×10^{-3}	2.64×10^{-3}	7.70×10^{3}	1.96
25		1.58	2.75	2.08	10.00	2.90
26		2.16	2.31	1.49	14.50	3.51
27		1.74	2.10	1.11	18.00	3.96
28		1.88	2.16	1.01	23.00	4.22
29		1.95	3.35	0.81	28.60	4.29
30		1.81	2.11	0.61	32.50	4.41

APPENDIX A: NOTATION

b	Width of ribbon; or half channel width
B	Width of channel, $B = 2b$
C	A constant relating to interface slope, Equation 1
C_D	Drag coefficient of ribbons
E	Modulus of elasticity of ribbon material
F_Δ	Densimetric Froude number; $F_\Delta^2 = \dfrac{U^2}{g(\Delta\rho_s/\rho)h_w}$
g	Acceleration due to gravity
h_s	Depth of saline water layer; interface heights
h_w	Depth of freshwater layer
H	Elevation of free surface measured from the channel bottom $H = h_s + h_w$
H_o, H_1	Elevation of free surface in the entrance and exit segments of channel
k	Optical manometer telescope indication, $k = 88\,\ell_c$
l_ρ	Effective thickness of interface layer based on densities as defined by Equation 26
l_u	Effective thickness of interface layer based on velocities as defined by Equation 33
L	Length of interface line between $x = 0$ and $x = x$; length of wires
p	Pressure
p_{xz}	Tangential stress on a plane normal to x-axis and in the direction of z-axis
p_{yx}, p_{yz}	Tangential stresses on a plane normal to y-axis in the directions of x- and z-axis, respectively
p_{zx}	Tangential stress on a plane normal to z axis and in the direction of x-axis
q	Freshwater discharge per unit width of channel
Q	Freshwater discharge, $Q = qB$
Q_{s1}	Volume of saline water entering into interface layer from saline water below $z = -\ell$
Q_{s2}	Volume of saline water entering into fresh water through interface layer upper boundary at $z = \ell_c/2$
R	Reynolds number Uh_w/ν; or telescope scale reading; or curvature of velocity meter ribbon at distance s; or effective resistance
R_i	Gross Richardson number defined by Equation 35
R_{io}	Interfacial Richardson number defined by Equation 36

AD-A155 010 AN EXPERIMENT IN MIXING AND INTERFACIAL STRESS(U) ARMY ENGINEER WATERWAYS EXPERIMENT STATION VICKSBURG MS HYDRAULICS LAB G H KEULEGAN FEB 85 WES/MP/HL-85-1 2/2

UNCLASSIFIED F/G 20/4 NL

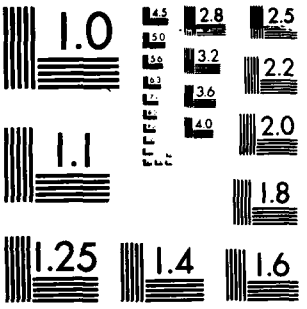

s	Distance measured along ribbon length; or the spacing between the wires of salinity measuring device; or the distance between the cylinders of the optical manometer
S	Distance of telescope scale from the manometer cells; or salinity
t	Thickness of ribbon
$\bar{u}$	Depth averaged of u for a given y along the depth h_w of freshwater layer
u_i, w_i	Horizontal and vertical velocity components, respectively, of interface points
u_m	Saline water mixing velocity at the interface
u_s	Current velocity at the freshwater free surface
u, w	Horizontal and vertical velocities at a point
U	Average value of $\bar{u}$, averaged over the channel width B; average velocity of flowing fresh water
U_c	Threshold critical velocity associated with the initiation of mixing
U_i, W_i	Average of values of u_i, w_i, respectively, averaged over the channel width B
U_m	Average of u_m, averaged across the channel width B; $U_m = U_{m1} + U_{m2}$
U_{m1}	Component part of transport defined by Q_{s1}/L where Q_{s1} denotes the volume of salt carried by the interface per unit time and L, the interface length
U_{m2}	Freshwater component defined by Q_{s2}/L, where Q_{s2} denotes the volume of salt carried by fresh water per unit time
U_s	Average value of u_s, averaged over the channel width B
x	Horizontal coordinate drawn in the direction of flow of fresh water
y	Horizontal coordinate drawn laterally with respect to channel walls
z	Elevation of points measured from the channel bottom
z'	Elevation of points in the freshwater layer measured from the interface line where $\Delta\rho/\rho_s = 0.5$
ℓ	Length of ribbon of velocity measuring device
α	Boussinesq coefficient of velocity distribution as in Equation 86; or a coefficient relating to salinity as in Equation 48; also specific ratio by mass for solutions as in Equation 46
β	Coefficient of velocity distribution in saline water as defined by Equation 95; or a coefficient relating to density distribution in freshwater layer as in Equation 39
δ	Fall of freshwater free surface; $H = H_o - \delta$
δ_c	Relative displacement of liquid surfaces in the two cells of the optical manometer

δ_o Lower bound of interfacial layer where $\Delta\rho/\Delta\rho_s = 0.99$

$\Delta\rho'$ Average value of $\Delta\rho$ in fresh water, averaged over depth h_w

$\Delta\rho_s$ Excess of density of saline water of lower layer over that of fresh water

ε Absorption contents in mixtures, Equation 47

λ_i Friction coefficient of interface as defined by Equation 108

λ_l Friction coefficient of wall of part in contact with saline water as defined by Equation 99

λ_o Friction coefficient of wall of part in contact with fresh water as defined by Equation 92

μ Coefficient of viscosity

ν Kinematic viscosity of water

ρ Density of fresh water

ρ_m Density of solute

τ Specific resistance of electrolyte in ohms, Equation 36

τ_o Bottom frictional stress; $\bar{\tau}_o$ average value averaged over the channel width B

τ_s Tangential stress at the interface; $\bar{\tau}_s$ average value averaged over the channel width B

τ_w Frictional stress of vertical walls; $\bar{\tau}_w$ averaged value; averaged separately over parts of wall in contact either with fresh water or saline water

Ω Volume of water

Ω_m Volume of solute

Ω_s Volume of solution


DAT
FILM